NASA TECHNICAL NOTE

NASA TN D-6802

NASA TN D-6802

DISCRETE SONIC JETS USED AS BOUNDARY-LAYER TRIPS AT MACH NUMBERS OF 6 AND 8.5

by David R. Stone and Aubrey M. Cary, Jr.

Langley Research Center
Hampton, Va. 23365

NATIONAL AERONAUTICS AND SPACE ADMINISTRATION • WASHINGTON, D. C. • JULY 1972

1. Report No.	2. Government Accession No.	3. Recipient's Catalog No.
NASA TN D-6802		

4. Title and Subtitle
DISCRETE SONIC JETS USED AS BOUNDARY-LAYER TRIPS AT MACH NUMBERS OF 6 AND 8.5

5. Report Date
July 1972

6. Performing Organization Code

7. Author(s)
David R. Stone and Aubrey M. Cary, Jr.

8. Performing Organization Report No.
L-8215

10. Work Unit No.
117-07-01-01

9. Performing Organization Name and Address
NASA Langley Research Center
Hampton, Va. 23365

11. Contract or Grant No.

13. Type of Report and Period Covered
Technical Note

12. Sponsoring Agency Name and Address
National Aeronautics and Space Administration
Washington, D.C. 20546

14. Sponsoring Agency Code

15. Supplementary Notes The material presented herein is based on a thesis by David Ray Stone entitled "The Effect of Discrete Jets Used as a Boundary Layer Trip on Transition, Heat Transfer, and the Downstream Flowfield at Mach Numbers of 6.0 and 8.5" submitted in partial fulfillment of the requirements for the degree of Master of Science, North Carolina State University, Raleigh, North Carolina, 1971.

16. Abstract

This experimental investigation shows the effect of discrete three-dimensional sonic jets used to promote transition on a sharp-leading-edge flat plate at Mach numbers of 6 and 8.5 and unit Reynolds numbers as high as 2.5×10^5 per cm in the Langley 20-inch hypersonic tunnels. An examination of the downstream flow-field distortions associated with the discrete jets for the Mach 8.5 flow was also conducted. Jet trips are found to produce lengths of turbulent flow comparable to those obtained for spherical-roughness-element trips while significantly reducing the downstream flow distortions. A Reynolds number based upon secondary jet penetration into a supersonic main flow is used to correlate jet-trip effectiveness just as a Reynolds number based upon roughness height is used to correlate spherical-trip effectiveness. Measured heat-transfer data are in agreement with the predictions based on the modified Spalding and Chi method.

17. Key Words (Suggested by Author(s))	18. Distribution Statement
Hypersonic boundary-layer trips Hypersonic boundary-layer profiles with trips Jet trips	Unclassified – Unlimited

19. Security Classif. (of this report)	20. Security Classif. (of this page)	21. No. of Pages	22. Price*
Unclassified	Unclassified	51	$3.00

*For sale by the National Technical Information Service, Springfield, Virginia 22151

DISCRETE SONIC JETS USED AS BOUNDARY-LAYER TRIPS AT MACH NUMBERS OF 6 AND 8.5*

By David R. Stone and Aubrey M. Cary, Jr.
Langley Research Center

SUMMARY

This experimental investigation shows the effect of discrete three-dimensional sonic jets used to promote transition on a sharp-leading-edge flat plate at Mach numbers of 6 and 8.5 and unit Reynolds numbers as high as 2.5×10^5 per cm in the Langley 20-inch hypersonic tunnels. An examination of the downstream flow-field distortions associated with the discrete jets for the Mach 8.5 flow was also conducted. Jet trips are found to produce lengths of turbulent flow comparable to those obtained for spherical-roughness-element trips while significantly reducing the downstream flow distortions. A Reynolds number based upon secondary jet penetration into a supersonic main flow is used to correlate jet-trip effectiveness just as a Reynolds number based upon roughness height is used to correlate spherical-trip effectiveness. Measured heat-transfer data are in agreement with the predictions based on the modified Spalding and Chi method.

INTRODUCTION

Turbulent flow has been observed over large portions of flight vehicles up to Mach 6 (ref. 1) and may be expected at even higher Mach numbers on proposed large vehicles such as the space shuttle and hypersonic transport. The relative low Reynolds numbers and high transition Reynolds numbers usually associated with high Mach number wind tunnels often necessitate using roughness trips to produce turbulent boundary-layer flow over most of the configuration. The most widely used means of producing turbulent flow on wind-tunnel models is the use of roughness elements such as sand grit, spherical balls, cylinders, and set screws as boundary-layer trips. At low hypersonic Mach numbers (up to Mach 6) roughness sizes required to move transition relatively close to the trips are approximately twice the height of the laminar boundary layer at the trip position (ref. 2).

*The material presented herein is based on a thesis by David Ray Stone entitled "The Effect of Discrete Jets Used as a Boundary Layer Trip on Transition, Heat Transfer, and the Downstream Flowfield at Mach Numbers of 6.0 and 8.5" submitted in partial fulfillment of the requirements for the degree of Master of Science, North Carolina State University, Raleigh, North Carolina, 1971.

For these relatively large trips it has been shown (ref. 3) that the accompanying element pressure drag is a substantial portion of the overall drag of the wind-tunnel model and is extremely difficult to determine accurately. For configuration testing at hypersonic speeds where drag measurement is a test output, extreme caution must be exercised if roughness trips are used to simulate turbulent flow conditions. Another investigation (ref. 4) has also shown that large distortions are found in the velocity field and outer portion of the boundary layer downstream of these large roughness elements. Thus, a configuration utilizing roughness trips ahead of control surfaces or engine inlets, for example, may not entirely simulate the results that would be obtained in a naturally turbulent flow.

Such disadvantages of conventional roughness trips suggest an examination of other means of tripping the hypersonic laminar boundary layer. Discharging air from small holes in the model surface was used to trip the laminar boundary layer at subsonic speeds by Fage and Sargent (ref. 5). Coles (ref. 6) also used sonic jets in the model surface as a tripping device at supersonic speeds to move transition forward of skin-friction measurement devices located on a flat plate. In this reference, it was pointed out that a most important property of discrete jets used as a tripping device, aside from the obvious advantage of control during the test, is the low intrinsic drag of the jets since the thrust component of the jet is initially discharged normal to the external flow. Coles as well as Korkegi (ref. 7) was successful in promoting early transition at supersonic speeds with discrete jets; however, their primary interest was in measuring turbulent skin friction.

Previously there was little information available for sizing discrete jets used as boundary-layer trips. Limited experimental data indicate that properly sized jet trips can promote transition in high-speed flow; however, a comparison of the effectiveness of jets in producing lengths of turbulent flow with that of the more conventional spherical-roughness trips does not exist. For hypersonic flow, effective spherical-element trips have been shown to cause large distortions of the downstream flow field (ref. 4); no information is presently available to indicate the effects of jet trips on the downstream flow field.

The purpose of the present experiment was to investigate the effectiveness of three-dimensional sonic jets injecting normal to the laminar boundary layer as a means of promoting transition. The experiments were conducted on a sharp-leading-edge flat plate at free-stream Mach numbers of 6 and 8.5. An examination of the downstream flow-field distortions associated with effective discrete jets for the Mach 8.5 flow was also conducted. A Reynolds number based upon jet penetration into a supersonic main flow is used to correlate jet trip effectiveness just as a Reynolds number based upon roughness height is used to correlate spherical-trip effectiveness. Transition locations are determined from heat-transfer distributions for various unit Reynolds numbers and injection rates. The measured heat-transfer rates are also compared with the turbulent heating rates predicted by using the modified Spalding-Chi method (refs. 8 and 9). Boundary-layer surveys (pitot

and total temperature) were obtained near adiabatic wall conditions for the naturally turbulent boundary layer and at two downstream locations directly behind discrete jets and spherical-roughness elements which were sized to promote transition to its most forward position relative to the trip location. A comparison of the tripped and untripped turbulent boundary layers is made by using conventional velocity profiles as well as profiles in temperature-velocity coordinates.

SYMBOLS

C	constant of proportionality in equation (8)
c_p	specific heat of air at constant pressure
c_m	specific heat of the model material
d	diameter of jet orifice
h	jet penetration parameter
k	height of spherical roughness element
M	Mach number
N_{St}	Stanton number, $\dfrac{\dot{q}}{\rho_\infty u_\infty c_p(T_{aw} - T_w)}$
p	absolute pressure
p_{probe}	pitot pressure measured by total-pressure probe
$\dot{q}$	surface heat-transfer rate
R	unit Reynolds number per cm, u/ν
R_h	jet-trip-height Reynolds number based on free-stream conditions, $u_\infty h/\nu_\infty$
R_k	spherical-trip-height Reynolds number based on free-stream conditions, $u_\infty k/\nu_\infty$
$R_{h,eff}$	effective jet-trip-height Reynolds number (see p. 14)

$R_{k,eff}$	effective spherical-trip-height Reynolds number (see p. 11)
R_x	Reynolds number based on chordwise distance from leading edge, $u_\infty x/\nu_\infty$
$R_{x,k}$	Reynolds number based on chordwise distance from leading edge to trip position, $u_\infty x_k/\nu_\infty$
$R_{x,t}$	Reynolds number based on chordwise distance from leading edge to end of induced transition, $u_\infty x_t/\nu_\infty$
$R_{x,v}$	Reynolds number based on distance from virtual origin, $u_\infty x_v/\nu_\infty$
r	recovery factor
s	lateral spacing between jet center lines
T	temperature
T_{probe}	temperature measured by total-temperature probe
t	time
u	velocity in x-direction
x,y,z	model coordinates (see fig. 2)
x_k	longitudinal distance from plate leading edge to trip location
x_t	longitudinal distance from plate leading edge to transition position
$x_{t,0}$	longitudinal distance from plate leading edge to natural transition
x_v	longitudinal distance along plate, measured from end of transition
y_0	Mach disk height
y_1	penetration above Mach disk
α	angle of attack

γ ratio of specific heats

δ boundary-layer thickness

θ momentum thickness

λ mass-flow parameter, $\dfrac{p_{t,j}\gamma_j}{p_\infty M_\infty{}^2\gamma_\infty}$

μ viscosity

ν kinematic viscosity, μ/ρ

ρ density

ϕ local skin thickness

Subscripts:

aw adiabatic wall

e conditions at edge of boundary layer

j conditions at jet exit plane

m model

t stagnation

w wall

∞ undisturbed free stream

APPARATUS AND TESTS

Tunnels

The test programs were conducted in the Langley 20-inch hypersonic tunnels (Mach 6 and 8.5). The wind tunnels are of the blowdown type exhausting through variable second minimums to either a 25 000-m^3 vacuum sphere or the atmosphere with the aid of

an annular ejector. The Mach 6 tunnel has a contoured nozzle with a rectangular test section 51 by 52 cm. Normal operating stagnation pressure can vary from approximately 3 to 37 atmospheres, and by using electrical heaters, stagnation temperatures up to 589 K can be obtained. The Mach 8.5 tunnel has an axially symmetric contoured nozzle with a test section 53 cm in diameter and can be operated at stagnation pressures of 34 to 170 atmospheres and stagnation temperatures up to 866 K. More detailed descriptions of these tunnels are given in reference 10.

The model injection system for the heat-transfer tests was located on top of the tunnels directly above the test section. A rectangular opening in top of the tunnel wall allowed the model to be injected to the center line of the test section for the Mach 6 tunnel and 5 cm above and 10 cm forward of the window center line for the Mach 8.5 tunnel. For the wall pressure data and flow-field surveys the flat plate was mounted on a rigid sting so that the test surface was 5 cm above the center line of the tunnel. The survey mechanism was located in the injector opening in the top of the tunnel above the test section. The leading edge of the model for the survey tests was located 30.5 cm forward of the center line of the window so that surveys could be obtained along most of the model length. The calibrations of the test core for the Mach 6 (ref. 11) and 8.5 (ref. 12) tunnels indicate that the free-stream Mach number for the present heat-transfer tests is 6.0 ± 0.02 and 8.45 ± 0.02, respectively.

Models and Instrumentation

Model 1.- The model used to obtain heat-transfer data at Mach 6.0 was a stainless-steel flat plate with a leading-edge bevel angle of 20° and a nose thickness of approximately 0.005 cm (see fig. 1). The air jets consisted of 9 holes drilled perpendicular to the model surface along a line 2.5 cm from the leading edge at a spacing of 0.64 cm between jet center lines (see insert in fig. 1). Air was supplied to each jet by a 0.23-cm-diameter tube which was connected to a common manifold fed by a line extending outside the tunnel to a 69 N/cm^2 supply line. The pressure in the manifold was controlled by a needle valve and measured by a 0 to 17 N/cm^2 strain-gage-type diaphragm pressure transducer. The instrumentation consisted of 30-gage iron-constantan thermocouples spotwelded to the undersurface of a 2.54-cm-wide slot along the plate center line (see table 1). The slot was milled to give an average surface skin thickness of 0.046 cm.

Model 2.- The model used to obtain heat-transfer data, wall pressure data, and flow-field surveys in the Mach 8.5 tunnel was a stainless-steel flat plate with a leading-edge bevel angle of 15° and a nose thickness of approximately 0.003 cm (see fig. 2). Two 0.318-cm-thick inserts for the plate were constructed from Inconel-600, one being instrumented with 0.23-cm-diameter pressure orifices and the other with 30-gage iron-constantan thermocouples (locations listed in table 2). The undersurface of the plate

instrumented with thermocouples was slotted along the center line to a width of 1.9 cm and a surface skin thickness of approximately 0.08 cm.

The air jets consisted of two rows of holes drilled perpendicular to the model surface at 2.5 and 7.6 cm from the leading edge. Each line contained 17 jets with the same dimensions as the jets for model 1. Air was supplied to each jet by a common manifold fed by a line extending outside the tunnel to a 690 N/cm^2 supply line. The pressure in the manifold was controlled by a needle valve and measured by three strain-gage-type diaphragm pressure transducers having ranges of 0 to 3.4, 0 to 17, and 0 to 69 N/cm^2.

To help provide a two-dimensional zero-pressure-gradient boundary layer along the test surface, end plates were attached to the models (see fig. 1). The leading-edge bevel angle of the end plates was 15^o and the edge thicknesses facing the flow were approximately 0.005 cm. The end plates were designed to enclose the leading-edge shock.

Survey probes and mechanism.- The survey probe mechanism which gave the probe two degrees of freedom in the xy-plane was driven by two electric motors. The vertical position of the probe was obtained by a precalibrated linear potentiometer which indicated the probe position with an accuracy of ±0.003 cm. The survey position along the x-direction was set before the test and the position of the model surface was indicated by electrical contact of the probe with the model after equilibrium conditions were established in the tunnel.

Schematics of the total-pressure and total-temperature probes are given in figures 3(a) and 3(b), respectively. The total-pressure probe was made of stainless-steel tubing flattened to a height of 0.025 cm with an opening height of 0.018 cm at the tip. The total-temperature probe was constructed from a swaged thermocouple silver-soldered into a stainless-steel tube of 0.19-cm outside diameter. The thermocouple consisted of 30-gage chromel-alumel wires welded at their junctions.

Test Conditions

The heat-transfer tests made in the Mach 6 tunnel were obtained over a stagnation-pressure range of 11.2 to 34.0 atmospheres at a stagnation temperature of approximately 533 K. These conditions correspond to free-stream unit Reynolds numbers from approximately 0.79×10^5 to 2.48×10^5 per cm.

The heat-transfer, pressure, and flow-field survey tests made in the Mach 8.5 tunnel were obtained at stagnation conditions which would give the highest unit Reynolds number for continuous operation and, therefore, produce the largest extent of naturally turbulent boundary layer flow over the model. The data were obtained at a stagnation pressure of approximately 136 atmospheres and at a stagnation temperature of 839 K corresponding to a free-stream unit Reynolds number of approximately 2.0×10^5 per cm.

DATA REDUCTION

Pressure Data

The pressures were measured with strain-gage-type diaphragm pressure transducers. Surface static pressures were measured with transducers having a range of 0 to 0.69 N/cm^2. The pitot survey probe was connected to three transducers having ranges of 0 to 0.69, 0 to 3.4, and 0 to 17 N/cm^2. The accuracy of all transducer readings was 0.25 percent of full-scale reading.

Total-Temperature Data

The electrical output of the total-temperature probe was monitored during the test runs and data were recorded when the output became steady at a given probe position. This probe has been calibrated at Mach numbers of 3, 6, and 8.5 through a wide range of Reynolds numbers and had a recovery factor $\frac{T_{probe} - T_e}{T_t - T_e}$ of approximately 1.0. A probe recovery factor of 1.0 was, therefore, assumed for all the present tests.

Heat-Transfer Data

The aerodynamic heating was determined by the thin-skin transient calorimetry technique by which the rate of heat storage in the model skin is measured. The models, initially at room temperature (approximately 305 K), were exposed to the airstream by rapid injection (0.25 second) from a shielded position. The electrical outputs from the thermocouples were sampled 20 times each second and were recorded on a high-speed digital recorder. When the model was positioned at rest in the test section, the temperature-time data for 1 second were fitted to a second-degree polynomial of the form

$$T_w = a + bt + ct^2 \tag{1}$$

where a, b, and c are constants. The time derivative of temperature used to calculate the heating coefficients was computed at the first point of the curve fit.

Because of the fast insertion into the test flow, the models were considered to have been subjected to a step function in aerodynamic convective heat input. Radiative heating for the most extreme conditions encountered in this investigation (tunnel wall temperature, 400 K; model wall temperature, 300 K) was negligible compared with the aerodynamic heating. Conduction heat-transfer error was calculated by using the three-point finite-difference method described in reference 13 for the most extreme conditions of measured spanwise and chordwise temperature gradients. Generally, the conduction heating was less than 1 percent of the convection heating; thus, no corrections for conduc-

tion were applied to the experimental data. With the assumption of no radiative and conductive heat losses, the local surface heating rate for the models is expressed as

$$\dot{q} = c_m \rho_m \phi \frac{dT_w}{dt} \tag{2}$$

where c_m is the specific heat of the model material in J/kg-K and is calculated from the following equation:

$$c_m = k_1 + k_2 T_w \tag{3}$$

ρ_m is the model density, and T_w in equation (3) is in K. The following constants were used for model 1: Type 405 stainless steel

$$k_1 = 290.4 \text{ J/kg-K}$$

$$k_2 = 0.558 \text{ J/kg-K}^2$$

$$\rho_m = 7737 \text{ kg/m}^3$$

and for model 2: Type Inconel-600

$$k_1 = 292.7 \text{ J/kg-K}$$

$$k_2 = 0.459 \text{ J/kg-K}^2$$

$$\rho_m = 8538 \text{ kg/m}^3$$

The Stanton number was based on free-stream conditions ahead of the model and was calculated from the equation

$$N_{St} = \frac{\dot{q}}{\rho_\infty u_\infty c_p \left(T_{aw} - T_w\right)} \tag{4}$$

where

$$T_{aw} = T_{\infty}\left[1 + rM_{\infty}^{2}\left(\frac{\gamma - 1}{2}\right)\right] \tag{5}$$

The recovery factor r was taken to be

$r = 0.845$ (Laminar)

$r = 0.890$ (Turbulent)

Determination of Transition

The method used in this investigation to determine the location of boundary-layer transition was by heat-transfer measurements. Whenever possible, the transition location x_t as used herein refers to the end of transition (peak heating). For the cases where the transition location approached the first thermocouple position (2.5 cm downstream of the jet), the movement of peak heating forward of this position could no longer be determined. Since it has been shown (refs. 14 and 15) that the most forward movement of induced transition does not occur at the trip position, it is herein assumed that transition occurs at the first thermocouple location whenever peak heating occurs at or forward of the first thermocouple location. This criterion will allow an analysis of the data which is believed to be adequate for most applications.

RESULTS AND DISCUSSION

Flow Visualization

Schlieren photographs of the models without end plates are shown in figure 4 alined at $\alpha = 0^{\circ}$. The angles between the leading-edge shock (or Mach) wave and the instrumented surface are approximately 10° and 8°, consistent with the calculated values for Mach 6.0 and 8.5, respectively. The apparent thickness of the leading-edge shock wave could be attributed to a small roll angle of the model relative to the coordinates of the schlieren system as well as to some diffraction. The jet bow shock had no observable effect on the leading-edge shock for the Mach 6.0 case. A detailed study of the shock patterns both with and without injection at Mach 8.5 indicated that the jets displaced the leading-edge shock slightly upward from the plate but did not significantly change the leading-edge shock angle downstream of the injection point.

Flow Field About Trips

An understanding of the flow field around and downstream of discrete jets and a comparison of the jet flow field with the flow field of the more conventional spherical-element trips are desirable to gain insight into the mechanisms by which jet trips promote transition. A schematic of the flow field about an underexpanded jet exhausting normal to a supersonic main flow is shown in figure 5. Similar flow models are presented in references 16 and 17. The disturbance created by the jet flow exhausting into the primary stream forms a bow shock upstream of the jet. The main flow separates well ahead of the jet due to the adverse pressure gradient created by the jet bow shock impinging on the boundary layer. The jet flow expands until a normal shock (Mach disk) produces a static pressure equal to the "ambient" pressure of the external flow at the jet boundary.

Surface oil-flow patterns obtained at Mach 8.5 for both spherical elements and discrete jets, shown in figure 6(a), suggest that the flow-field characteristics about both trips are similar. A flow model for the spherical elements was proposed in reference 15 and is shown in figure 6(b). The traces on the oil-flow patterns for the spherical elements suggest that vortex filaments are present near the surface ahead of and around the sphere. It appears that spherical-roughness-induced transition results from disturbances introduced by these vortices. Although the exact mechanism by which transition occurs is not known, the vortices may break down and introduce turbulence directly into the boundary layer as suggested by Hall (ref. 18) for incompressible flow and Van Driest and McCauley (ref. 19) for supersonic speeds.

Surface oil-flow patterns obtained by using discrete jets, shown in figure 6(a), indicate the presence of vortex patterns similar to those obtained for spherical elements. Korkegi (ref. 7) investigated the mechanism by which jet trips promote transition by using a luminescent-lacquer technique; traces in the lacquer were interpreted as being two spiral vortices generated on either side of the air jet. These vortices induce boundary-layer transition downstream of the jet. The proposed flow model for spherical elements, shown in figure 6(b), could be considered similar to the flow model for discrete jets presented in figure 5, where the sphere diameter has been replaced by the jet protuberance (or jet boundary).

Required Trip Size

Guidelines for choosing effective spherical-roughness trips (reviewed in ref. 15) utilize the roughness-height Reynolds number R_k as an important correlation parameter. By placing roughness elements far forward of natural transition and increasing R_k beyond some minimum value, transition moves rapidly forward until, finally, further increases in R_k result in only a slight movement of transition. The value of R_k for which further increases in R_k result in only slight movement in transition is taken to be the effective value, designated $R_{k,eff}$. Figure 7 shows the effect of both trip-

position Reynolds number $R_{x,k}$ and Mach number on the effective trip Reynolds number $R_{k,eff}$ for spherical-roughness-induced transition on flat plates where all nonadiabatic data have been adjusted to adiabatic wall conditions by using the Van Driest equation (ref. 15). This figure was taken from reference 15, with the exception of the solid symbol which represents data obtained by the authors of the present paper.

Because of the similarity of the jet- and spherical-trip flow fields, it is reasonable to assume that an equivalent jet-trip height can be used as a correlation parameter for jet-trip effectiveness in a manner similar to the sphere height k being used to correlate roughness-induced transition. Studies using secondary injection of highly underexpanded gases into a supersonic main flow (refs. 16, 17, 20, and 21) define various jet heights which could be used in a correlation for jet-trip effectiveness based on a height parameter associated with the penetration of jets into the main flow. Schetz and Billig (ref. 17) divided the penetration of the jet into two parts (see fig. 5): the distance to the Mach disk y_0 and the penetration above the Mach disk y_1. Zukoski and Spaid (ref. 20) established a theoretical penetration height parameter h for sonic jets based on a force balance between the jet momentum flux and the axial force exerted on a spherical-shaped surface of height equal to h. This parameter is given by the following equation:

$$\frac{h}{d} = K\left(M_\infty, \gamma_j, \frac{p_{t,j}}{p_\infty}\right)\lambda^{1/2} \tag{6}$$

where λ is a mass-flow parameter related to the ratio of sonic jet momentum flux to free-stream dynamic pressure and is written

$$\lambda = \frac{p_{t,j}\gamma_j}{p_\infty M_\infty{}^2 \gamma_\infty} \tag{7}$$

and K is expressed as a weak function of Mach number, γ_j, and pressure ratio $p_{t,j}/p_\infty$. Calculations for air over a range of Mach numbers up to 8.5 and pressure ratios from 10 to 1000 indicate that the value of K is approximately unity. Schlieren photographs taken by Zukoski and Spaid of secondary injection up to Mach 4.5 indicated that the theoretical penetration height parameter h corresponded closely to the Mach disk height y_0. Theoretical values of h as well as measured Mach disk heights for Mach numbers up to 4.5 (refs. 20 and 21) are shown in figure 8 as h/d plotted as a function of λ. Both Torrence (ref. 16) and Zukoski and Spaid (ref. 20) measured penetration of the jet $y_0 + y_1$ by the use of a tracer gas. Concentration measurements as far as 30 jet diameters downstream of injection indicated that the major strength of the jet (highest concentration level) was located near the Mach disk height with maximum penetration occurring a few jet

diameters downstream of the injection point. Torrence's empirical correlation (see fig. 8) for maximum jet penetration was also found to be a function of $\lambda^{1/2}$ and was approximately 3.5 times the Mach disk height.

Since both the maximum jet penetration and jet Mach disk height are approximately proportional to $\lambda^{1/2}$ for all the available data, an equivalent-jet-trip-height parameter h could be introduced where

$$\frac{h}{d} = C\lambda^{1/2} \tag{8}$$

For the value of h to correspond directly to spherical-trip heights, the constant C should probably be chosen such that h would fall somewhere between the Mach disk height and the maximum jet penetration height.

Effects of Discrete Jets on Boundary-Layer Transition and Heat-Transfer Distributions

In figures 9 and 10, the distributions of surface heating in the form of Stanton numbers along the plate for various jet mass injection rates are presented for free-stream Mach numbers of 6.0 and 8.5, respectively. The location of transition x_t has been identified in the figure for each injection rate.

Comparison of heat-transfer distributions with theory.- Calculated variations of Stanton number with Reynolds number for laminar and turbulent regions of the boundary layer obtained by use of the Monaghan T' (ref. 22) and the modified Spalding and Chi (refs. 8 and 9) methods, respectively, are shown for comparison with data in figures 9 and 10. Calculations of laminar heat transfer based on the Monaghan T' method were in good agreement with the untripped data (fig. 9(a)). Untripped turbulent heating rates were slightly underpredicted but were, on the average, within 10 percent of the modified Spalding-Chi (S-C) theory based on free-stream conditions and with the virtual origin chosen as the point of peak heating x_t. Similar agreement with the modified Spalding-Chi theory was obtained for the jet-tripped turbulent flow at both Mach numbers. At Mach 6.0 where transition occurred close to the trip location, the use of the virtual origin based on the trip location was equally effective in predicting the turbulent heating rates downstream of the trip.

The model used for the Mach 8.5 tests was instrumented with rows of thermocouples between jet orifices. Spanwise differences in surface heating rates were sometimes noted downstream of injection as indicated in figure 10(b); however, once turbulent flow had been obtained no consistent spanwise differences in the heating-rate distributions were observed.

Movement of transition.- The movement of transition is given in figure 11(a) for various injection rates and unit Reynolds numbers at Mach 6.0 and in figure 11(b) for various injection rates and two trip locations at Mach 8.45; the data are listed in table 3. At Mach 6.0 the most forward transition location was within 2.5 cm of the trip location, with resulting transition Reynolds numbers $R_{x,t}$ as low as 4.0×10^5. For the Mach 8.5 flow the most forward transition location was approximately 8 to 10 cm downstream of the trip location, with resulting transition Reynolds numbers as low as 2.5×10^6. This increase in transition Reynolds number with Mach number is not unexpected since it was indicated in reference 15 that for spherical-roughness-induced transition the difference between the transition Reynolds number and the trip-position Reynolds number $R_{x,t} - R_{x,k}$ for effective trips increases with Mach number.

The movement of transition at given injection rates for two different jet spacings is shown in figure 11(a) for the Mach 6.0 flow. Increasing the jet spacing had negligible effect on the transition position downstream of the jet-orifice center line. This is similar to the effect of spacing found for spherical-roughness-induced transition (ref. 15) where an increase in spacing from 4 to 8 times the sphere diameter had little effect on transition position. However, a jet spacing should be chosen that would give a uniform transition location across the width of the model.

Transition correlation.- The variation of jet-induced transition location with jet-height Reynolds number R_h is presented in figure 12 for Mach numbers of 6.0 and 8.5. The data are presented in a form similar to that used for spherical roughness in reference 15. For reasons of simplicity C in equation (8) was chosen to be unity such that

$$\frac{h}{d} \equiv \lambda^{1/2} \tag{9}$$

By using $C = 1$, the equivalent jet-trip height will be approximately the height of the Mach disk. A dimensionless parameter referenced to the distance between natural transition and the trip location $\frac{x_t - x_k}{x_{t,0} - x_k}$ has been used to represent the movement of transition relative to the trip location. A value of this parameter of 1.0 would represent no movement of transition whereas a value of zero would mean that transition had moved to the trip location. Similar to the method outlined in reference 15, the bend (or knee) in the transition curve represents the effective trip $R_{h,eff}$ for that position Reynolds number as indicated in figure 12.

The movement of transition for spherical elements with the spherical-roughness Reynolds number R_k is also shown in figure 12 at similar values of $R_{x,k}$ for both Mach 6.0 and 8.5. Although the relative movement of transition with R_k could be made to coincide with that of R_h, the values of R_k and R_h were not the same. Also at

Mach 8.5 where jet-induced transition did not occur close to the trip location, both types of trips produced comparable lengths of turbulent flow. The movement of transition with trip Reynolds number is a further indication of the similarity that exists between jet trips and spherical elements.

Figure 13 shows the effect of both Mach number and $R_{x,k}$ on $R_{h,eff}$ for the data of the present investigation as well as adiabatic wall data taken from references 6 and 7. The nonadiabatic wall data of the present investigation have been adjusted to adiabatic wall conditions by using the Van Driest equation (ref. 15) developed for spherical roughness by replacing k with the equivalent jet-trip height h calculated from equation (9). The movement of jet-induced transition with jet mass flow for references 6 and 7 was obtained from skin-friction measurements taken at fixed locations downstream of the jet trip. The effective Reynolds number $R_{h,eff}$ was determined from the jet mass flow for which the skin friction at the measuring station first became constant.

In figure 13(a), $R_{h,eff}$ was found to increase with increasing values of $R_{x,k}$ with the greatest rate of increase at the higher Mach numbers. Figure 13(b) shows the growth of $R_{h,eff}$ with Mach numbers up to 8.5 for the ranges of $R_{x,k}$ available. It appears from this analysis that the trends found for jet-induced transition are similar to those previously found for spherical roughness elements (fig. 7). Also, for the range of data presented in this investigation the criterion for specifying the jet strength necessary for effective tripping can be conditionally established by the use of figure 13 combined with the Van Driest equation for the wall cooling effect and equation (9) for the required value of λ.

It is of interest to note that for effective tripping (compare fig. 13 and fig. 7) as well as for the same relative movement of transition (see fig. 12), the required value of R_k was approximately 3.5 to 4.0 times that of R_h where h was taken as the Mach disk height (eq. (9)). By assuming that the magnitudes of jet penetration found for supersonic flow up to Mach 4.5 (given in fig. 8) can be extended to hypersonic Mach numbers, the equivalent jet-trip height closely corresponding to the effective spherical-roughness height would be the maximum jet-penetration height. It is therefore inferred that effective jet trips could be approximately sized for flow conditions outside the range of this investigation by the use of spherical-roughness-induced-transition data where the maximum jet-penetration height is used for the jet-trip height.

Comparison of Downstream Flow-Field Properties

Flow-field surveys behind effective spherical roughness elements at Mach 8.5 have shown the [illegible] distortions in the outer boundary layer and inviscid flow field downstream of the rough[illegible] can occur; therefore, an experimental investigation of the flow field downstream of effective jet trips was undertaken. The present flow-field surveys

required long test times; thus, the model surface temperature for the surveys $\left(\frac{T_w}{T_t} \approx 0.7\right)$ was higher than for the heat-transfer measurements $\left(\frac{T_w}{T_t} = 0.4\right)$. The criterion used to determine the effective jet trip at this higher wall-temperature level was based on the data from figure 13 combined with the Van Driest equation for the wall cooling effect. The value of $R_{h,eff}$ was increased 10 percent above the calculated value to insure turbulent flow from the most forward position possible.

Total-pressure and total-temperature surveys were taken at two positions downstream of the trip locations for effective jet and spherical trips. Typical wall static pressures used to reduce the pitot pressures to Mach number and surface temperature distributions are shown in figure 14. Weak shock waves present in the nozzle flow accounted for the variation in measured surface pressures shown in figure 14(a) found both with and without trips; however, the average change in local Mach number is less than 0.2 along the length of the plate. As seen in figure 14(b), a ratio of wall to total temperature of 0.7 can be assumed as a good approximation of the temperature level measured along the surface of the plate during the surveys.

Mach number profiles were obtained downstream of effective jet and spherical trips (fig. 15). The local Mach number was determined from the measured pitot and wall static pressures by assuming that the static pressure was constant normal to the wall. Since the static pressure between the boundary layer and the leading-edge shock is probably not constant, the Mach number profiles shown in figure 15 above the boundary layer can be used for comparative purposes only. Also shown in figure 15(a) are the no-roughness profile (for comparison of the inviscid flow) taken at $x = 27.9$ cm and a naturally turbulent boundary-layer profile with approximately the same turbulent Reynolds number $R_{x,v}$ taken at $x = 45.5$ cm. All transition locations for the surveys were determined from heat-transfer measurements. Included in figure 15(b) is the no-roughness profile taken at $x = 45.5$ cm; however, no naturally turbulent boundary-layer profile was obtained for comparison since the large turbulent Reynolds number for the tripped profiles could not be attained.

The inviscid flow field downstream of the jet trips at the first survey position (fig. 15(a)) is essentially the same as the flow field of the no-roughness case. Although the inviscid portion of the flow field for the smaller spherical roughness placed nearer the leading edge of the plate indicates somewhat smaller flow-field disturbances than for the spherical trip placed at the larger x_k, neither spherical trip simulates the natural inviscid flow field as well as the jet trip. These flow-field distortions produced by the spherical elements dissipate farther downstream of the roughness; for example, profiles taken at $R_{x,v} = 6.8 \times 10^6$ ($x = 45.5$ cm), presented in figure 15(b), indicate no significant

distortions remaining in the inviscid flow field except for the larger spherical trip. However, this profile position is beyond the region of interest for many tests utilizing trips.

A comparison of the turbulent boundary layer by using conventional velocity profiles (calculated from the measured Mach number and temperature profiles presented in table 4) for two survey positions is shown in figure 16 where the vertical distance has been nondimensionalized by experimental momentum thickness θ. Again, the profile utilizing jet trips better simulates the no-roughness profile taken at the same turbulent Reynolds number, especially in the outer regions of the boundary layer. Boundary-layer velocity profiles obtained at the rearward position (fig. 16(b)) downstream of the spherical elements were almost the same as the profile for the jet trips taken at approximately the same location.

Since the main objective of using trips is to produce a turbulent boundary layer which is the same as a naturally turbulent boundary layer at the same value of $R_{x,v}$, comparisons of the jet-tripped profiles with naturally turbulent profiles are of particular interest. An additional method of comparison is shown in figure 17 where the boundary-layer profiles are compared in temperature-velocity coordinates. All the profiles approximate an empirical quadratic relationship in the outer region and approach the linear Crocco relationship near the wall. The tripped and untripped profiles at almost the same value of $R_{x,v}$ are in good agreement. Whereas the tripped profile for the rearward position is slightly less full than the other profiles, this profile corresponds to a much higher turbulent Reynolds number.

Flat-plate temperature profiles measured at near-adiabatic wall conditions for Mach numbers of 3 to 10.5, reported in references 23 and 24, were scattered around the linear Crocco relation, and the sizable departure of the present profiles, both tripped and untripped, from this relation is unexpected. It is possible that the weak waves which influence the wall pressure distribution can also influence the temperature profile; however, at high Mach numbers the quadratic relationship of temperature and velocity may be realistic since the available higher Mach number data of reference 4 as well as the data of Softley and Sullivan (ref. 25) at Mach 10 follow the quadratic relation. The resolution of this question awaits the availability of additional high Mach number data obtained on flat plates.

CONCLUSIONS

An experimental investigation of discrete three-dimensional sonic jets injecting normal to the laminar boundary layer as a means of promoting early transition has been conducted on a sharp-leading-edge flat plate. At Mach 6 the Reynolds number range was 0.79×10^5 to 2.48×10^5 per cm, and at Mach 8.5 the Reynolds number was approximately 2.0×10^5 per cm. An examination of the downstream flow-field distortions associated

with the discrete jets for the Mach 8.5 flow was also conducted. The major conclusions derived from this study are as follows:

(1) Reynolds numbers based on the end of transition as low as 4.0×10^5 were obtained with air injection for the Mach 6 flow and as low as 2.5×10^6 at Mach 8.5. For both Mach numbers, jet trips produced lengths of turbulent flow that were comparable to those previously obtained for spherical roughness elements.

(2) A Reynolds number based on jet penetration into a supersonic main flow was found to correlate jet-trip effectiveness just as a Reynolds number based on roughness height correlated spherical-trip effectiveness. The effective jet-trip-height Reynolds number increased with increasing Mach number and trip-position Reynolds number in a manner similar to the increase for spherical-element trips. For the present test conditions, the correlations for the effects of spherical-roughness-induced transition can be used to size jet trips if the equivalent jet-trip height is taken to be the maximum jet-penetration height found for supersonic flow.

(3) Downstream flow distortions were significantly less for an effective jet trip than for the effective spherical-element trip required to produce the same transition position.

(4) With the virtual origin chosen as the point of peak heating at the end of transition, the heat-transfer data obtained for the jet-induced turbulent flow at both Mach 6 and 8.5 were in agreement with predictions of the modified Spalding and Chi theory.

Langley Research Center,
National Aeronautics and Space Administration,
Hampton, Va., June 16, 1972.

REFERENCES

1. Banner, Richard D.; and Kuhl, Albert E.: A Summary of X-15 Heat-Transfer and Skin-Friction Measurements. NASA TM X-1210, 1966.

2. Holloway, Paul F.; and Sterrett, James R.: Effect of Controlled Surface Roughness on Boundary-Layer Transition and Heat Transfer at Mach Numbers of 4.8 and 6.0. NASA TN D-2054, 1964.

3. Whitehead, Allen H., Jr.: Flow-Field and Drag Characteristics of Several Boundary-Layer Tripping Elements in Hypersonic Flow. NASA TN D-5454, 1969.

4. Morrisette, E. Leon; Stone, David R.; and Cary, Aubrey M., Jr.: Downstream Effects of Boundary-Layer Trips in Hypersonic Flow. Compressible Turbulent Boundary Layers, NASA SP-216, 1969, pp. 437-453.

5. Fage, A.; and Sargent, R. F.: An Air-Injection Method of Fixing Transition From Laminar to Turbulent Flow in a Boundary Layer. R. & M. No. 2106, Brit. A.R.C., 1944.

6. Coles, Donald: Measurements in the Boundary Layer on a Smooth Flat Plate in Supersonic Flow – III. Measurements in a Flat-Plate Boundary Layer at the Jet Propulsion Laboratory. Rep. No. 20-71 (Contract No. DA-04-495-Ord 18), Jet Propulsion Lab., California Inst. Technol., June 1, 1953.

7. Korkegi, Robert H.: Transition Studies and Skin-Friction Measurements on an Insulated Flat Plate at a Mach Number of 5.8. J. Aeronaut. Sci., vol. 23, no. 2, Feb. 1956, pp. 97-107, 192.

8. Spalding, D. B.; and Chi, S. W.: The Drag of a Compressible Turbulent Boundary Layer on a Smooth Flat Plate With and Without Heat Transfer. J. Fluid Mech., vol. 18, pt. 1, Jan. 1964, pp. 117-143.

9. Bertram, Mitchel H.; Cary, Aubrey M., Jr.; and Whitehead, Allen H., Jr.: Experiments With Hypersonic Turbulent Boundary Layers on Flat Plates and Delta Wings. AGARD CP No. 30, May 1968, pp. 1-1 – 1-21.

10. Schaefer, William T., Jr.: Characteristics of Major Active Wind Tunnels at the Langley Research Center. NASA TM X-1130, 1965.

11. Cary, Aubrey M., Jr.: Turbulent Boundary Layer Heat Transfer and Transition Measurements With Extreme Surface Cooling in Hypersonic Flow. M.A.E. Thesis, Univ. of Virginia, 1969.

12. Stone, David Ray: The Effect of Discrete Jets Used as a Boundary Layer Trip on Transition, Heat Transfer, and the Downstream Flowfield at Mach Numbers of 6.0 and 8.5. M.S. Thesis, North Carolina State Univ., 1971.

13. Bertram, Mitchel H.; and Everhart, Philip E.: An Experimental Study of the Pressure and Heat-Transfer Distribution on a 70° Sweep Slab Delta Wing in Hypersonic Flow. NASA TR R-153, 1963.

14. Van Driest, E. R.; and Blumer, C. B.: Boundary-Layer Transition at Supersonic Speeds – Three-Dimensional Roughness Effects (Spheres). J. Aerospace Sci., vol. 29, no. 8, Aug. 1962, pp. 909-916.

15. Morrisette, E. Leon; Stone, David R.; and Whitehead, Allen H., Jr.: Boundary-Layer Tripping With Emphasis on Hypersonic Flows. Viscous Drag Reduction, C. Sinclair Wells, ed., Plenum Press, 1969, pp. 33-51.

16. Torrence, Marvin G.: Concentration Measurements of an Injected Gas in a Supersonic Stream. NASA TN D-3860, 1967.

17. Schetz, Joseph A.; and Billig, Frederick S.: Penetration of Gaseous Jets Injected Into a Supersonic Stream. J. Spacecraft & Rockets, vol. 3, no. 11, Nov. 1966, pp. 1658-1665.

18. Hall, Gordon R.: Interaction of the Wake From Bluff Bodies With an Initially Laminar Boundary Layer. AIAA Paper No. 66-126, Jan. 1966.

19. Van Driest, E. R.; and McCauley, W. D.: The Effect of Controlled Three-Dimensional Roughness on Boundary-Layer Transition at Supersonic Speeds. J. Aero/Space Sci., vol. 27, no. 4, Apr. 1960, pp. 261-271, 303.

20. Zukoski, Edward E.; and Spaid, Frank W.: Secondary Injection of Gases Into a Supersonic Flow. AIAA J., vol. 2, no. 10, Oct. 1964, pp. 1689-1696.

21. Schetz, Joseph A.; Hawkins, Paul F.; and Lehman, Harry: Structure of Highly Underexpanded Transverse Jets in a Supersonic Stream. AIAA J., vol. 5, no. 5, May 1967, pp. 882-884.

22. Monaghan, R. J.: An Approximate Solution of the Compressible Laminar Boundary Layer on a Flat Plate. R. & M. No. 2760, Brit. A.R.C., 1953.

23. Bertram, Mitchel H.; and Neal, Luther, Jr.: Recent Experiments in Hypersonic Turbulent Boundary Layers. Presented at the AGARD Specialists Meeting on Recent Developments in Boundary-Layer Research (Naples, Italy), May 1965. (Also available as NASA TM X-56335.)

24. Bushnell, Dennis M.; Johnson, Charles B.; Harvey, William D.; and Feller, William V.: Comparison of Prediction Methods and Studies of Relaxation in Hypersonic Turbulent Nozzle-Wall Boundary Layers. Compressible Turbulent Boundary Layers, NASA SP-216, 1969, pp. 345-376.

25. Softley, Eric J.; and Sullivan, Robert J.: Theory and Experiment for the Structure of Some Hypersonic Boundary Layers. AGARD CP No. 30, May 1968, pp. 3-1 – 3-18.

TABLE 1.- THERMOCOUPLE LOCATIONS FOR MODEL 1

Thermocouple	x, cm	Thermocouple	x, cm
1	5.08	25	24.13
2	5.72	26	24.77
3	6.35	27	25.40
4	6.98	28	26.04
5	7.62	29	26.67
6	8.26	30	27.31
7	8.89	31	27.94
8	9.53	32	28.58
9	11.43	33	30.48
10	12.07	34	31.12
11	12.70	35	31.75
12	13.34	36	32.39
13	13.97	37	33.02
14	14.61	38	33.66
15	15.24	39	34.29
16	15.88	40	34.93
17	17.78	41	36.83
18	18.42	42	37.47
19	19.05	43	38.10
20	19.69	44	38.74
21	20.32	45	39.37
22	20.96	46	40.01
23	21.59	47	40.64
24	22.23	48	41.28

TABLE 2.- LOCATION OF MODEL INSTRUMENTATION FOR MODEL 2

Thermocouple locations					
Thermocouple	x, cm	z, cm	Thermocouple	x, cm	z, cm
1	5.08	0	49	48.90	0
2	5.72		50	50.17	0
3	6.35		51	6.02	-.159
4	6.98		52	7.92	
5	8.26		53	9.83	
6	8.89		54	11.73	
7	9.53		55	13.64	
8	10.16		56	15.54	
9	10.80		57	17.45	
10	11.43		58	19.35	
11	12.07		59	21.26	
12	12.70		60	23.16	
13	13.34		61	25.07	
14	13.97		62	5.08	-.318
15	14.61		63	6.98	
16	15.24		64	8.89	
17	15.88		65	10.80	
18	16.51		66	12.70	
19	17.15		67	14.61	
20	17.78		68	16.51	
21	18.42		69	18.42	
22	19.05		70	20.32	
23	19.69		71	22.23	
24	20.32		72	24.13	
25	20.96		73	27.94	
26	21.59		74	31.75	
27	22.23		75	35.56	
28	22.86		76	39.37	
29	23.50		77	43.18	
30	24.77		78	46.99	
31	25.40		79	6.02	-.635
32	26.04		80	7.92	
33	27.94		81	22.53	
34	28.58		82	11.73	
35	29.85		83	13.64	
36	31.12		84	15.54	
37	32.39		85	17.45	
38	34.93		86	19.35	
39	36.20		87	21.26	
40	37.47		88	23.16	
41	39.37		89	26.04	
42	40.01		90	29.85	
43	41.28		91	33.66	
44	42.55		92	37.47	
45	43.82		93	41.28	
46	45.09		94	45.09	
47	46.36		95	48.90	
48	47.63				

Pressure-orifice locations		
Pressure orifice	x, cm	z, cm
1	5.72	0
2	6.98	
3	8.26	
4	9.53	
5	10.80	
6	12.07	
7	13.34	
8	14.61	
9	15.88	
10	17.15	
11	19.05	
12	26.67	
13	34.29	
14	41.91	
15	49.53	
16	6.35	-.635
17	8.89	
18	11.43	
19	12.70	
20	13.97	
21	16.51	
22	17.78	
23	19.69	
24	24.13	
25	31.75	
26	39.37	
27	46.99	
28	5.72	1.588
29	6.98	
30	8.26	
31	10.80	
32	12.07	
33	13.34	
34	15.88	
35	17.15	
36	19.05	

Thermocouple locations for pressure insert		
Thermocouple	x, cm	z, cm
1	16.76	-1.778
2	27.94	
3	48.51	

TABLE 3.- SUMMARY OF TRANSITION LOCATIONS FOR VARIOUS MASS INJECTION RATES

Symbol (fig. 11)	M_∞	p_∞, N/cm^2	$p_{t,j}$, N/cm^2	x_t, cm	R_∞/cm	λ
○	6.0	0.0724	Natural transition	29.21	0.83×10^5	-----
		.0731	0.952	22.86	.83	0.36
		.0752	2.013	15.24	.87	.75
		.0745	2.117	14.61	.83	.79
		.0745	2.717	13.34	.83	1.01
●		.0731	3.627	11.43	.79	1.38
○		.0731	3.503	10.80	.83	1.33
		.0731	4.137	10.16	.83	1.58
		.0717	4.833	6.99	.87	1.88
		.0710	5.578	5.08	.75	2.18
●		.0752	6.261	5.08	.83	2.32
		.0738	9.798	5.08	.83	3.68
□		.1351	Natural transition	20.57	1.54	-----
		.1310	.855	16.51	1.49	.18
		.1303	1.979	10.80	1.49	.42
		.1296	1.979	10.16	1.49	.42
		.1310	3.537	7.62	1.49	.75
■		.1323	4.006	7.62	1.42	.84
□		.1310	4.116	6.99	1.49	.87
		.1310	5.571	5.08	1.49	1.18
■		.1345	6.509	5.08	1.49	1.35
		.1331	9.874	5.08	1.54	2.06
◇		.2165	Natural transition	16.51	2.48	-----
		.2123	1.083	11.43	2.44	.14
		.2130	2.013	7.62	2.44	.26
◆		.2186	3.834	6.99	2.48	.49
◇		.2117	3.454	6.35	2.40	.45
		.2172	4.082	5.08	2.48	.52
◆		.2186	6.599	5.08	2.44	.84
◇		.2103	9.667	5.08	2.36	1.28
◆		.2172	9.798	5.08	2.44	1.26
○	8.45	.0993	Natural transition	28.58	2.05	-----
		.0986	1.848	22.86	2.01	.26
		.0979	2.413	20.96	2.01	.34
		.0979	3.544	17.15	2.01	.51
		.0979	6.998	12.70	2.01	1.00
		.0986	10.343	12.70	2.01	1.48
		.0972	31.028	12.70	1.97	4.46
□		.1006	41.267	17.78	2.05	5.76
		.0993	66.344	15.24	2.05	9.39
		.0986	75.845	15.24	2.05	10.74

TABLE 4.- DATA FROM BOUNDARY-LAYER SURVEYS

(a) Profile 1

Trip	x_k, cm	Survey position, cm
None	----	45.5

$p_{t,\infty} = 1351$ N/cm^2, $T_{t,e} = 833$ K, $M_e = 7.82$

y, cm	p_{probe}, N/cm^2	M/M_e	$T_{probe}/T_{t,e}$	u/u_e
0	-----	0	[a] 0.728	0
.018	0.265	.152	[b] .816	.442
.019	.292	.164	[b] .820	.468
.028	.311	.169	[b] .840	.485
.038	.720	.258	.858	.646
.077	1.408	.395	.896	.797
.112	1.842	.454	.909	.839
.152	2.114	.487	.913	.857
.188	2.355	.515	.916	.870
.240	2.781	.561	.920	.889
.305	3.215	.604	.924	.904
.347	3.618	.641	.928	.915
.410	4.143	.687	.933	.928
.450	4.506	.716	.937	.935
.508	5.035	.757	.943	.945
.556	5.620	.801	.948	.954
.622	6.306	.849	.957	.964
.699	7.068	.899	.966	.974
.751	7.546	.929	.973	.981
.817	8.021	.958	.982	.988
.867	8.323	.976	.989	.992
.913	8.480	.985	.994	.996
.989	8.634	.995	.998	.998
1.055	8.705	.999	.999	.999
1.110	8.721	1.000	1.000	1.000

[a] Wall temperature.

[b] Extrapolated values of total temperature.

TABLE 4.- DATA FROM BOUNDARY-LAYER SURVEYS – Continued

(b) Profile 2

Trip	x_k, cm	Survey position, cm
Jets (λ = 2.5)	2.54	27.9

$p_{t,\infty}$ = 1379 N/cm^2, $T_{t,e}$ = 844 K, M_e = 7.74

y, cm	p_{probe}, N/cm^2	M/M_e	$T_{probe}/T_{t,e}$	u/u_e
0	-----	0	[a] 0.677	0
.018	0.292	.155	[b] .800	.440
.036	.439	.200	[b] .820	.537
.071	1.194	.346	.866	.744
.076	1.459	.385	.870	.777
.112	1.807	.430	.887	.814
.130	2.038	.457	.892	.831
.150	2.150	.468	.897	.839
.178	2.314	.487	.901	.850
.201	2.479	.503	.903	.858
.224	2.650	.519	.905	.865
.246	2.852	.538	.907	.873
.272	3.080	.561	.911	.883
.297	3.246	.583	.914	.891
.323	3.485	.607	.917	.900
.368	3.904	.644	.922	.912
.399	4.185	.667	.925	.918
.450	4.552	.695	.930	.927
.462	4.928	.725	.931	.933
.493	5.337	.754	.934	.939
.531	5.807	.787	.938	.946
.556	6.188	.813	.942	.952
.587	6.600	.840	.945	.957
.632	7.271	.883	.951	.965
.645	7.951	.898	.953	.967
.714	8.679	.939	.967	.978
.759	8.683	.964	.977	.985
.934	9.284	.999	.999	.999
1.196	9.308	1.000	1.000	1.000

[a] Wall temperature.

[b] Extrapolated values of total temperature.

TABLE 4.- DATA FROM BOUNDARY-LAYER SURVEYS – Continued

(c) Profile 3

Trip	x_k, cm	Survey position, cm
Sphere, k = 0.15 cm	1.27	27.9

$p_{t,\infty}$ = 1379 N/cm^2, $T_{t,e}$ = 833 K, M_e = 7.55

y, cm	p_{probe}, N/cm^2	M/M_e	$T_{probe}/T_{t,e}$	u/u_e
0	-----	0	[a] 0.700	0
.018	0.188	.109	[b] .832	.327
.051	.502	.224	[b] .887	.592
.079	.850	.299	.903	.704
.097	1.069	.338	.907	.746
.122	1.289	.373	.911	.783
.152	1.439	.395	.913	.797
.174	1.503	.404	.914	.804
.196	1.586	.416	.915	.812
.226	1.672	.427	.917	.820
.251	1.795	.442	.920	.831
.269	1.868	.450	.922	.836
.300	2.202	.469	.925	.848
.328	2.152	.483	.928	.856
.353	2.294	.500	.931	.865
.376	2.475	.519	.933	.874
.406	2.703	.544	.936	.886
.429	2.875	.562	.938	.893
.460	3.158	.586	.941	.903
.489	3.447	.613	.944	.913
.503	3.592	.626	.946	.914
.538	4.040	.664	.949	.928
.554	4.240	.682	.950	.934
.582	4.702	.716	.951	.940
.607	5.075	.743	.953	.944
.632	5.523	.774	.954	.952
.655	5.943	.804	.956	.957
.678	6.309	.828	.957	.960
.709	6.922	.869	.960	.968
.739	7.460	.902	.965	.973
.843	8.184	.944	.983	.986
.973	8.563	.967	.992	.993
1.135	9.067	1.000	1.000	1.000

[a] Wall temperature.

[b] Extrapolated values of total temperature.

TABLE 4.- DATA FROM BOUNDARY-LAYER SURVEYS – Continued

(d) Profile 4

Trip	x_k, cm	Survey position, cm
Sphere, k = 0.30 cm	4.45	27.9

$p_{t,\infty}$ = 1379 N/cm^2, $T_{t,e}$ = 833 K, M_e = 7.54

y, cm	p_{probe}, N/cm^2	M/M_e	$T_{probe}/T_{t,e}$	u/u_e
0	-----	0	[a] 0.700	0
.018	0.170	.098	[b] .813	.295
.041	.241	.142	[b] .858	.417
.071	.609	.253	.890	.639
.094	.808	.296	.903	.700
.124	1.069	.343	.912	.753
.155	1.213	.367	.916	.776
.198	1.365	.389	.921	.796
.221	1.441	.400	.923	.805
.254	1.579	.419	.926	.819
.269	1.620	.431	.927	.827
.297	1.751	.441	.929	.835
.330	1.889	.459	.932	.846
.358	2.034	.477	.934	.856
.378	2.151	.491	.936	.864
.404	2.292	.505	.938	.871
.429	2.503	.526	.940	.881
.465	2.737	.549	.943	.891
.521	3.137	.587	.947	.906
.546	3.365	.609	.950	.914
.572	3.565	.618	.952	.917
.620	3.971	.662	.957	.931
.686	4.482	.683	.963	.946
.734	4.599	.704	.965	.956
.787	4.992	.743	.974	.959
.820	5.157	.755	.977	.972
.975	5.847	.798	.988	.979
1.031	6.543	.841	.991	.985
1.079	7.115	.875	.993	.990
1.280	8.756	.970	.998	.996
1.400	9.267	1.000	1.000	1.000

[a] Wall temperature.

[b] Extrapolated values of total temperature.

TABLE 4.- DATA FROM BOUNDARY-LAYER SURVEYS – Continued

(e) Profile 5

Trip	x_k, cm	Survey position, cm
Jet (λ = 2.5)	2.54	45.5

$p_{t,\infty}$ = 1372 N/cm^2, $T_{t,e}$ = 833 K, M_e = 7.78

y, cm	p_{probe}, N/cm^2	M/M_e	$T_{probe}/T_{t,e}$	u/u_e
0	----	0	[a]0.693	0
.018	0.216	.129	[b].800	.380
.028	.279	.155	[b].817	.447
.068	.665	.262	.857	.649
.102	1.086	.341	.870	.742
.152	1.342	.382	.884	.781
.206	1.568	.412	.886	.803
.254	1.731	.437	.897	.823
.325	2.099	.482	.907	.851
.406	2.446	.522	.919	.874
.467	2.840	.563	.928	.893
.526	3.212	.599	.934	.906
.577	3.542	.631	.938	.917
.655	4.058	.676	.944	.930
.714	4.466	.712	.948	.939
.759	4.795	.737	.951	.945
.838	5.375	.782	.955	.954
.917	6.000	.828	.960	.963
.978	6.458	.860	.967	.970
1.039	6.957	.892	.974	.977
1.080	7.271	.913	.977	.981
1.118	7.504	.927	.981	.984
1.166	7.789	.945	.986	.988
1.214	8.035	.960	.990	.992
1.250	8.154	.967	.993	.994
1.493	8.481	.988	.999	.999
1.740	8.676	1.000	1.000	1.000

[a] Wall temperature.

[b] Extrapolated values of total temperature.

TABLE 4.- DATA FROM BOUNDARY-LAYER SURVEYS – Continued

(f) Profile 6

Trip	x_k, cm	Survey position, cm
Sphere, k = 0.15 cm	1.27	45.5

$p_{t,\infty}$ = 1382 N/cm^2, $T_{t,e}$ = 836 K, M_e = 7.80

y, cm	p_{probe}, N/cm^2	M/M_e	$T_{probe}/T_{t,e}$	u/u_e
0	----	0	[a]0.730	0
.018	0.164	.109	[b].823	.335
.048	.293	.172	[b].870	.499
.071	.514	.240	.890	.630
.109	.917	.328	.903	.743
.123	1.017	.347	.905	.762
.145	1.149	.370	.909	.783
.170	1.220	.383	.912	.794
.195	1.291	.395	.913	.803
.221	1.365	.406	.914	.811
.249	1.448	.418	.915	.820
.300	1.614	.442	.918	.835
.366	1.837	.474	.924	.854
.399	1.951	.489	.926	.862
.447	2.150	.514	.931	.875
.498	2.387	.542	.935	.888
.561	2.643	.572	.940	.900
.617	2.965	.605	.944	.912
.675	3.302	.638	.947	.922
.731	3.663	.672	.950	.931
.782	4.037	.706	.953	.940
.810	4.256	.725	.954	.943
.869	4.704	.760	.958	.951
.912	5.105	.792	.962	.958
.988	5.718	.838	.970	.968
1.097	6.481	.893	.986	.982
1.189	6.964	.926	.990	.987
1.308	7.543	.964	.994	.993
1.422	7.894	.986	.997	.997
1.519	8.177	1.000	1.000	1.000

[a] Wall temperature.

[b] Extrapolated values of total temperature.

TABLE 4.- DATA FROM BOUNDARY-LAYER SURVEYS – Concluded

(g) Profile 7

Trip	x_k, cm	Survey position, cm
Sphere, k = 0.30 cm	4.45	45.5

$p_{t,\infty}$ = 1375 N/cm^2, $T_{t,e}$ = 840 K, M_e = 7.87

y, cm	p_{probe}, N/cm^2	M/M_e	$T_{probe}/T_{t,e}$	u/u_e
0	----	0	[a]0.720	0
.018	0.160	.091	[b].789	.276
.068	.243	.140	[b].873	.429
.089	.456	.209	.891	.582
.170	1.034	.328	.916	.752
.183	1.168	.351	.917	.774
.234	1.282	.367	.921	.788
.300	1.539	.400	.924	.806
.338	1.593	.410	.925	.822
.424	2.015	.469	.929	.858
.480	2.151	.479	.934	.864
.546	2.603	.535	.941	.891
.640	3.047	.573	.948	.908
.681	3.447	.620	.950	.921
.767	3.861	.648	.958	.932
.805	4.337	.696	.959	.942
.932	5.626	.796	.967	.962
1.039	6.653	.866	.974	.974
1.163	7.453	.917	.980	.984
1.288	7.970	.953	.991	.992
1.430	8.377	.976	.995	.995
1.537	8.522	.984	.996	.996
1.676	8.694	.994	.999	.999
1.796	8.784	1.000	1.000	1.000

[a] Wall temperature.

[b] Extrapolated values of total temperature.

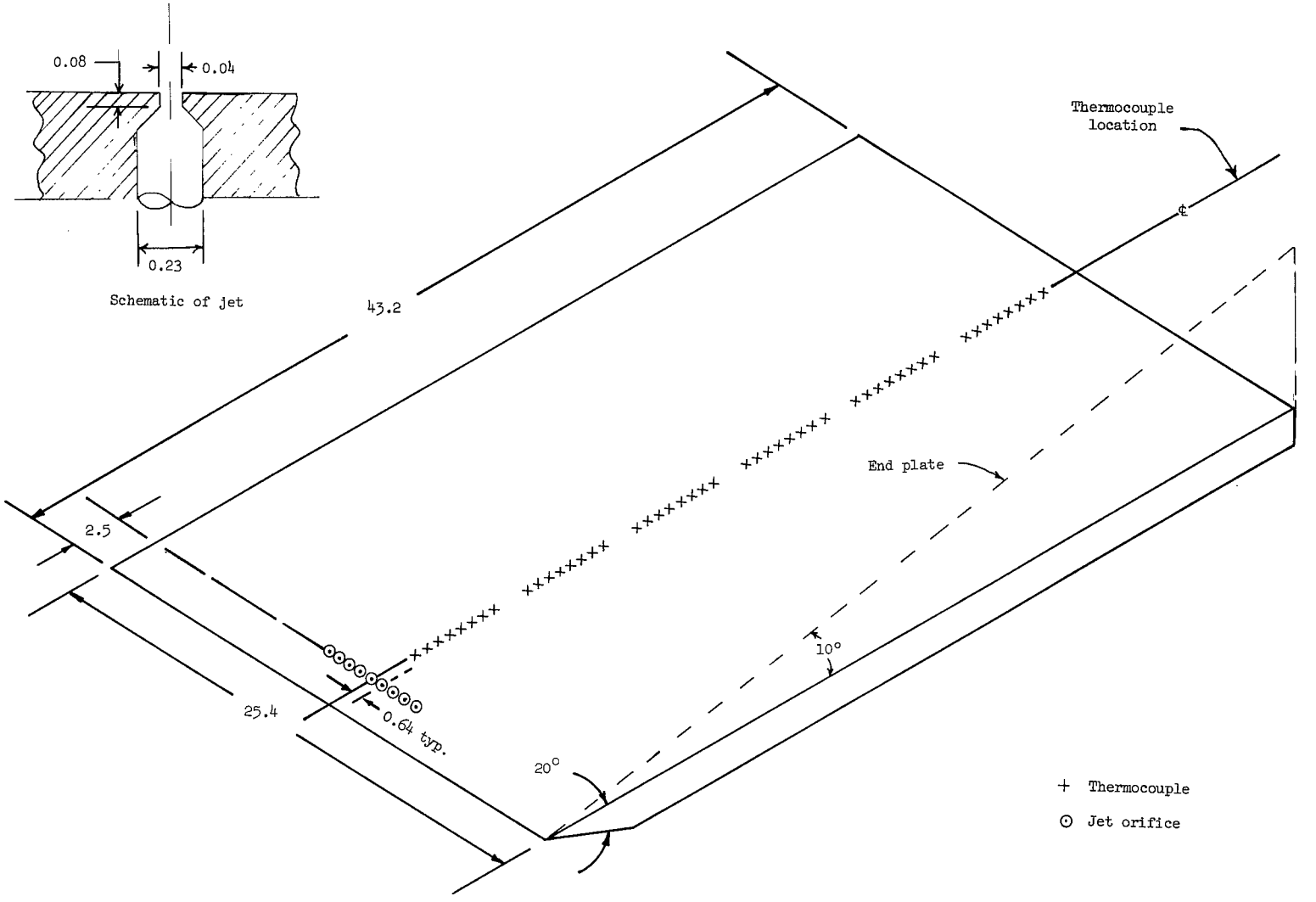

Figure 1.- Flat-plate heat-transfer assembly, model 1. All dimensions are in centimeters.

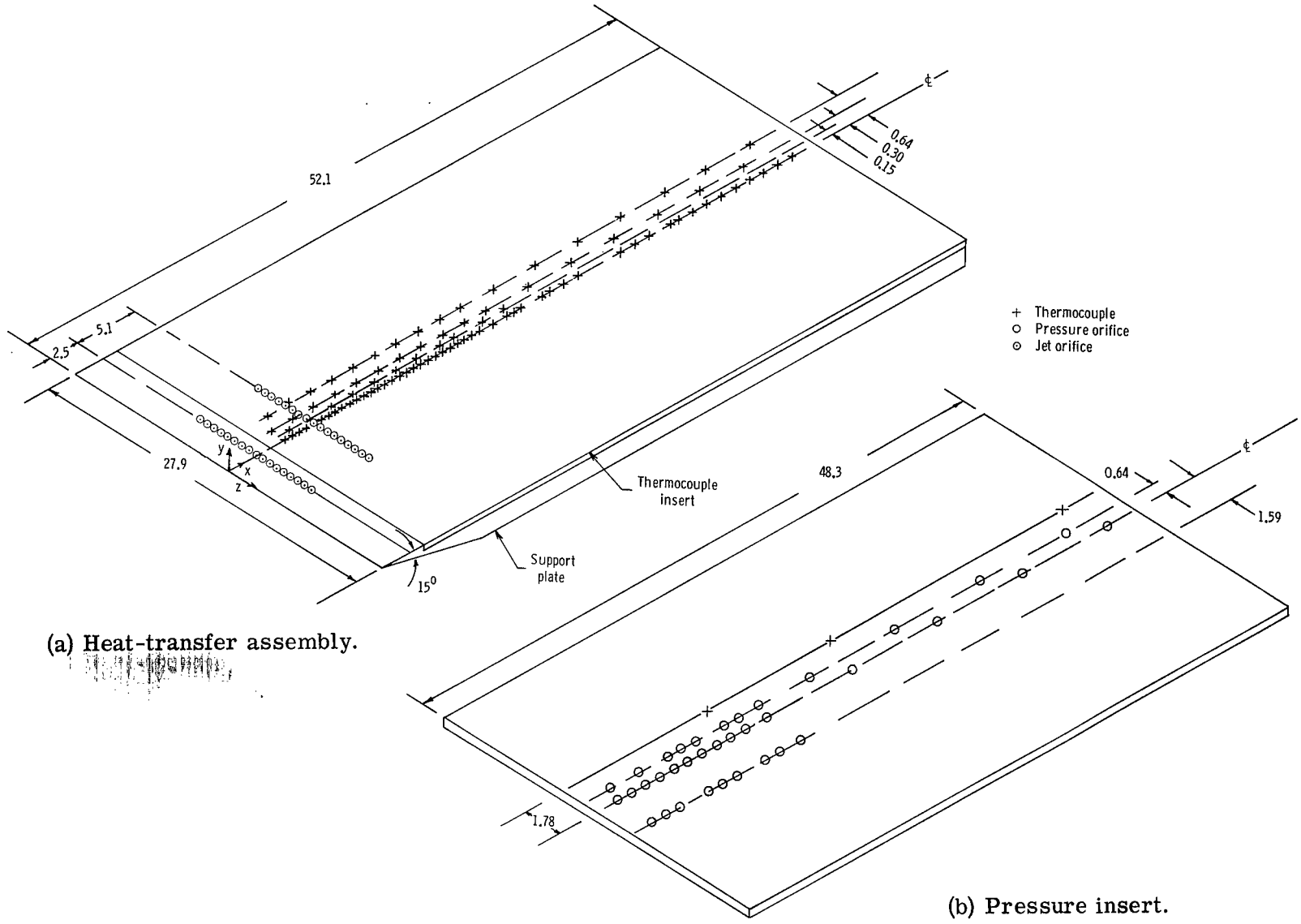

(a) Heat-transfer assembly.

(b) Pressure insert.

Figure 2.- Flat-plate assembly, model 2. All dimensions are in centimeters.

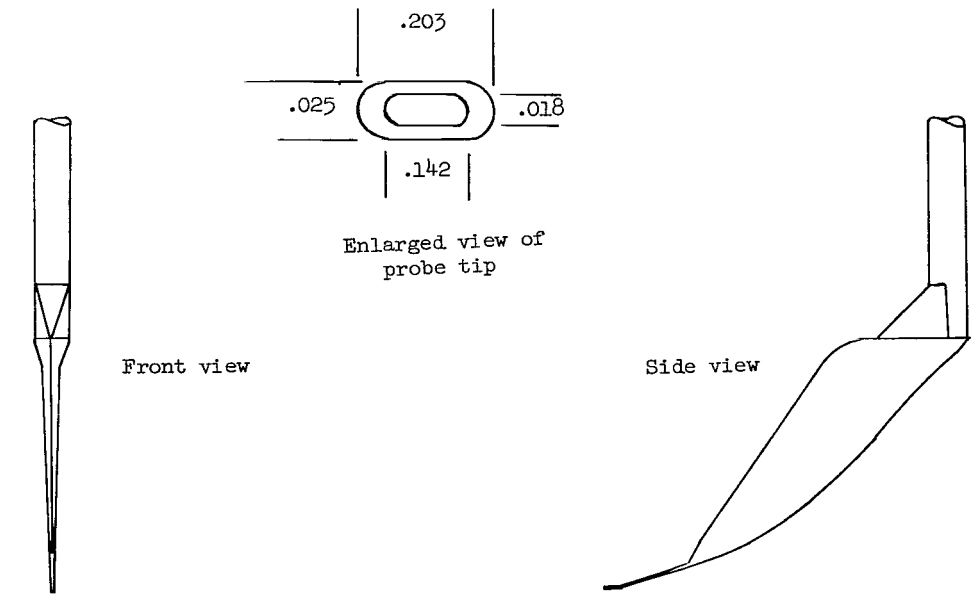

(a) Total-pressure probe.

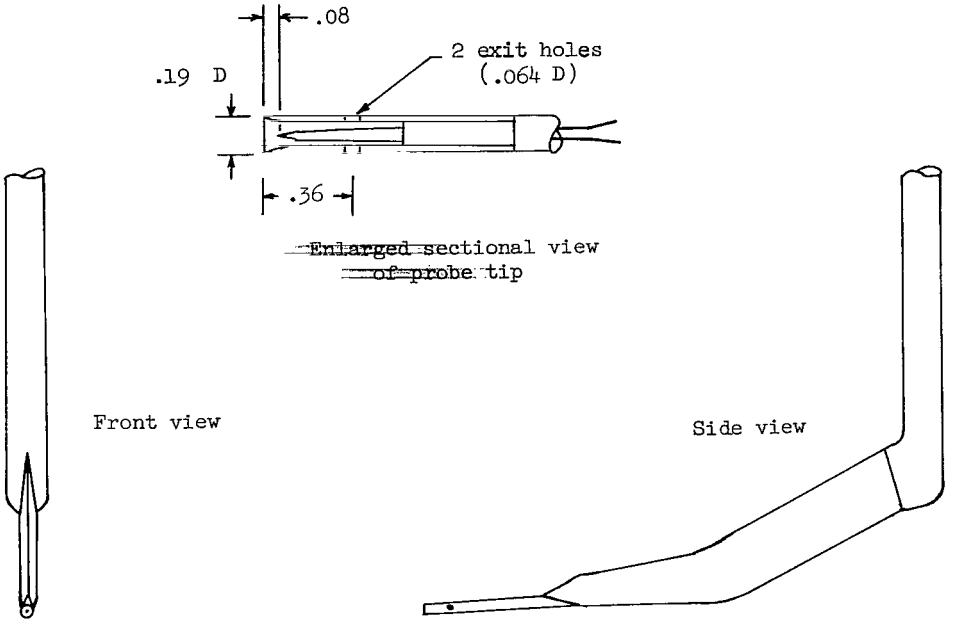

(b) Total-temperature probe.

Figure 3.- Schematic drawings of probes. All dimensions are in centimeters.

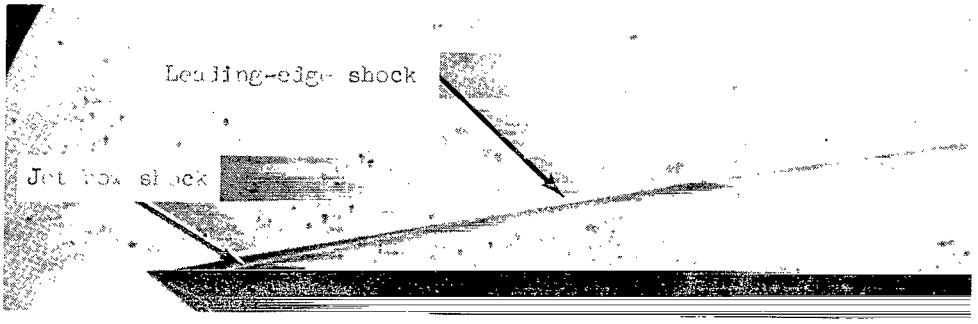

(a) Mach 6.0; $p_{t,j}/p_\infty = 57.0$; $R_{x,k} = 2.0 \times 10^5$.

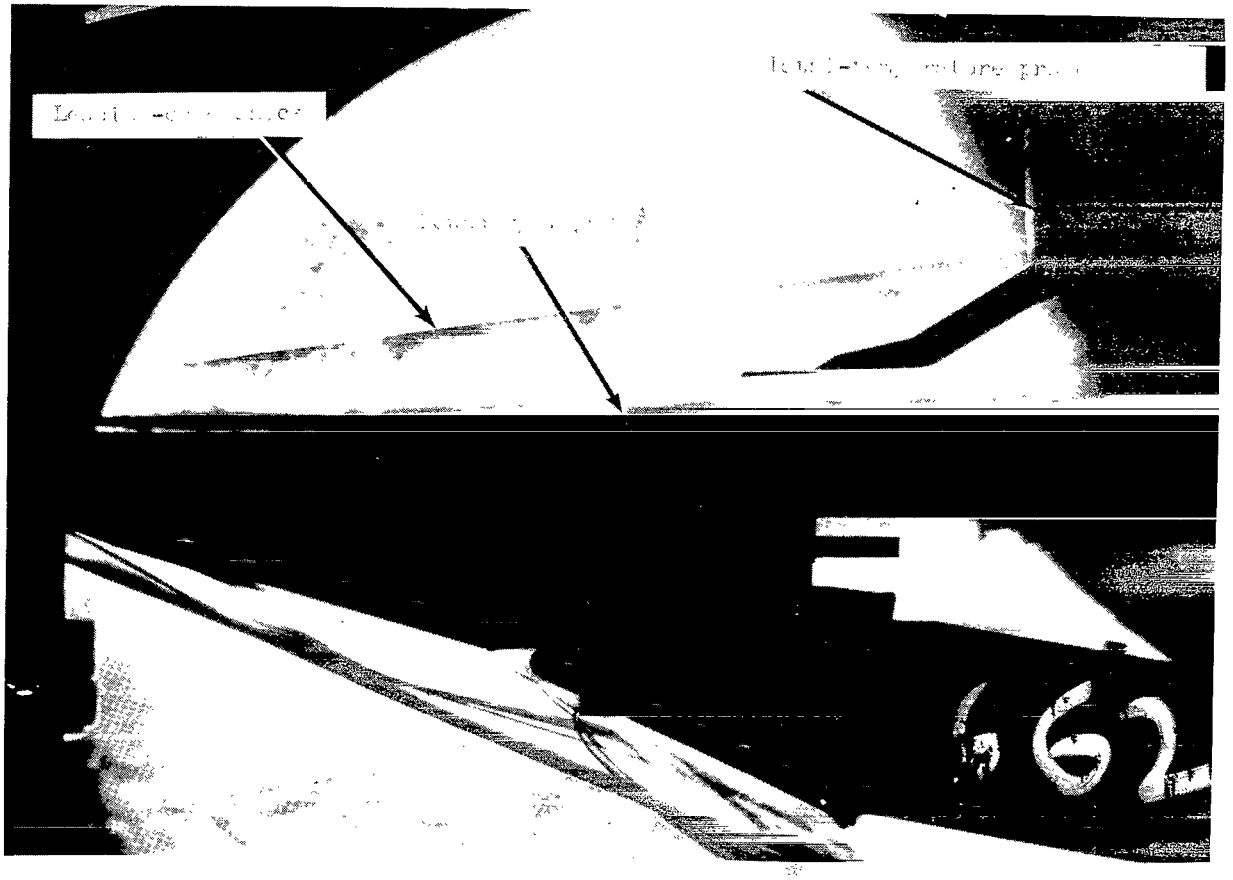

(b) Mach 8.5; $p_{t,j}/p_\infty = 180.0$; $R_{x,k} = 5.2 \times 10^5$.

Figure 4.- Schlieren photographs showing flow details and model orientation.

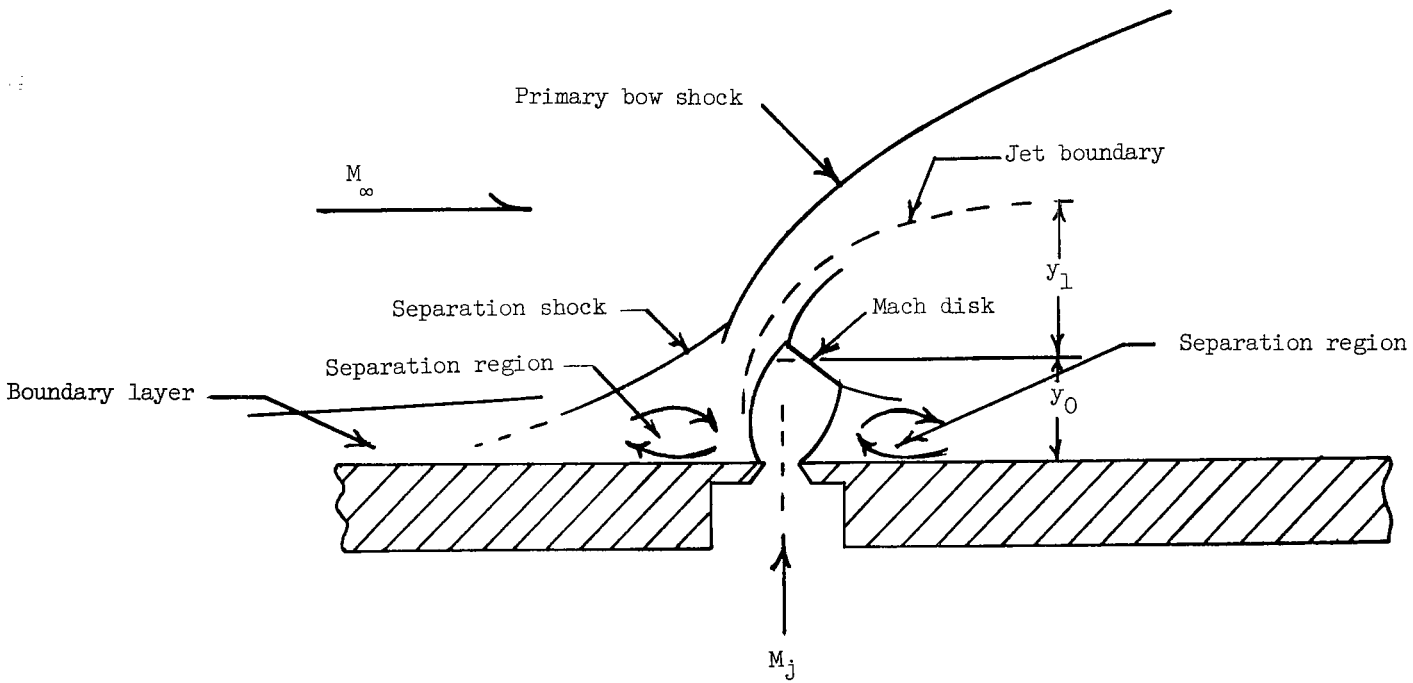

Figure 5.- Schematic of flow field about an underexpanded jet normal to a supersonic flow.

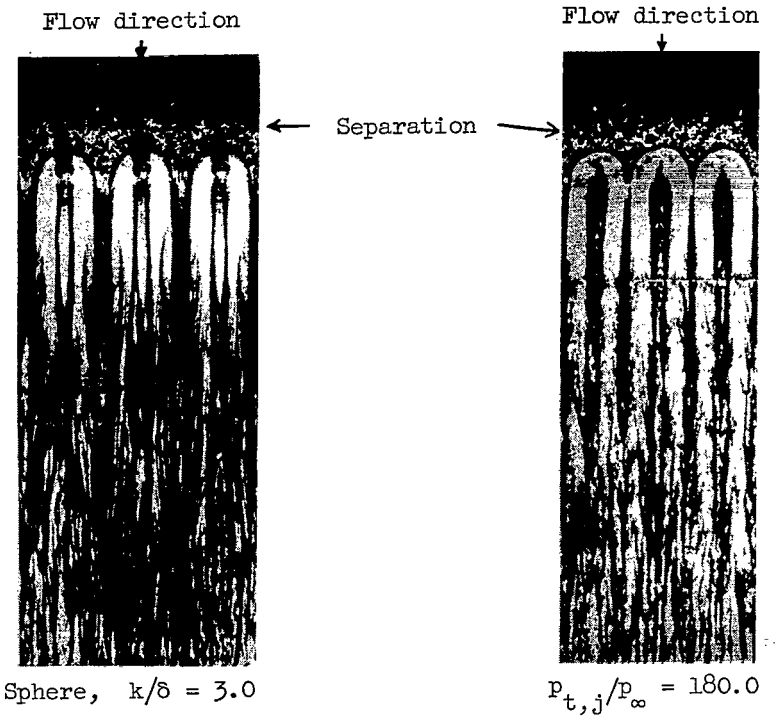

(a) Oil-flow photographs. $M_\infty = 8.5$; $R_{x,k} = 5.2 \times 10^5$; $T_w/T_t = 0.40$.

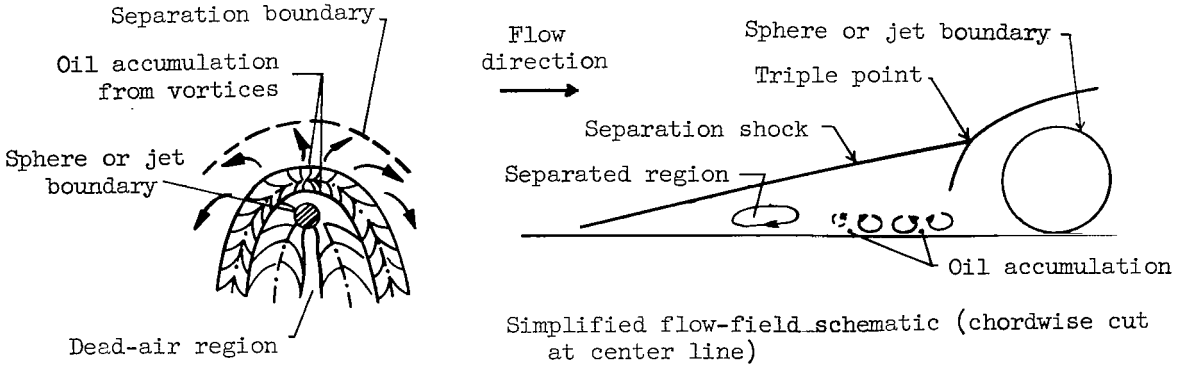

(b) Interpretation.

Figure 6.- Comparison of flow field about discrete jet or spherical-element trip.

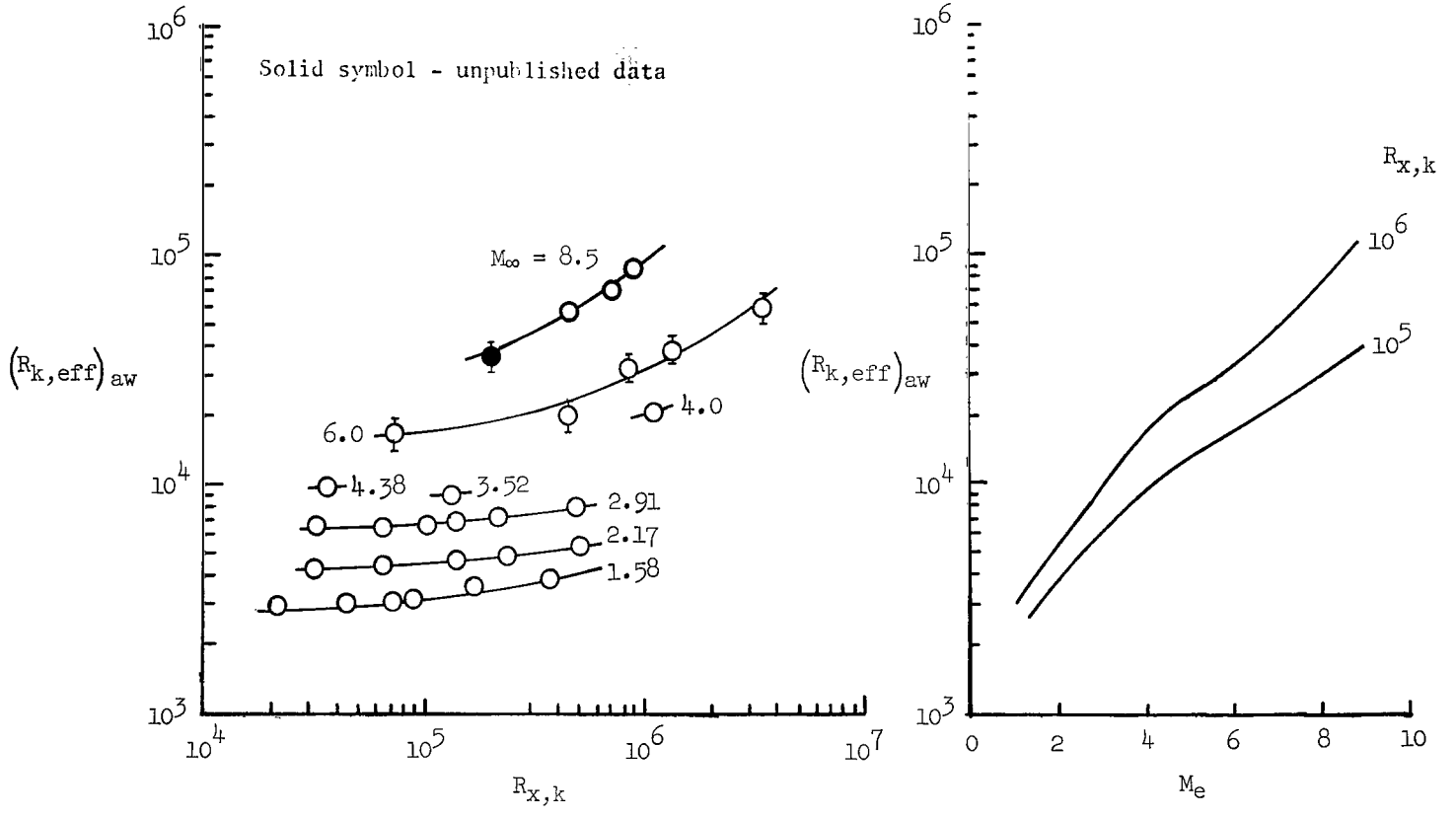

(a) Constant Mach number.

(b) Constant $R_{x,k}$.

Figure 7.- Variation of effective roughness Reynolds number with roughness-position Reynolds number and Mach number for spherical roughness elements at adiabatic wall conditions. (Taken from ref. 15, except solid symbol.)

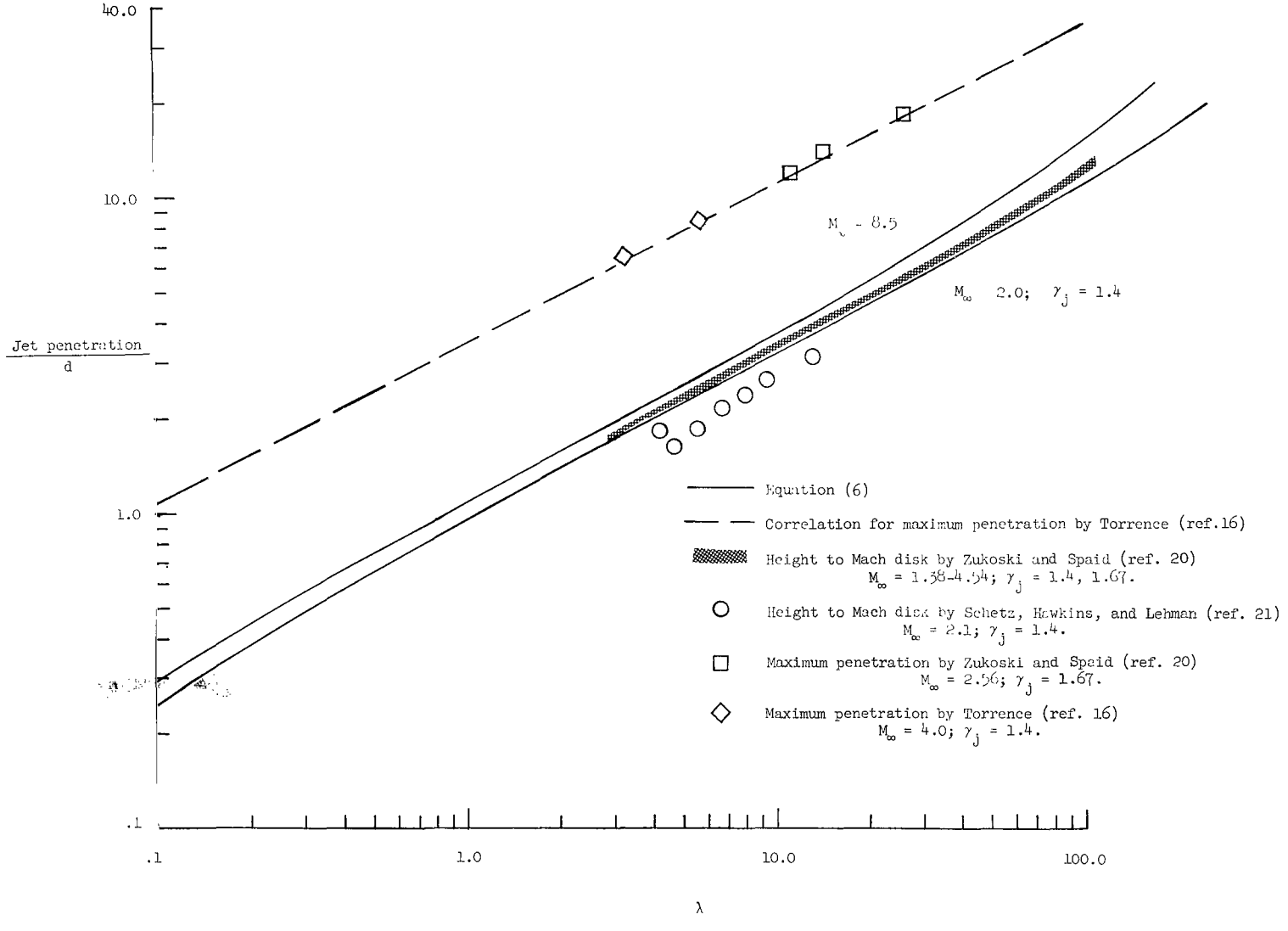

Figure 8.- Penetration of underexpanded jets in supersonic main flow.

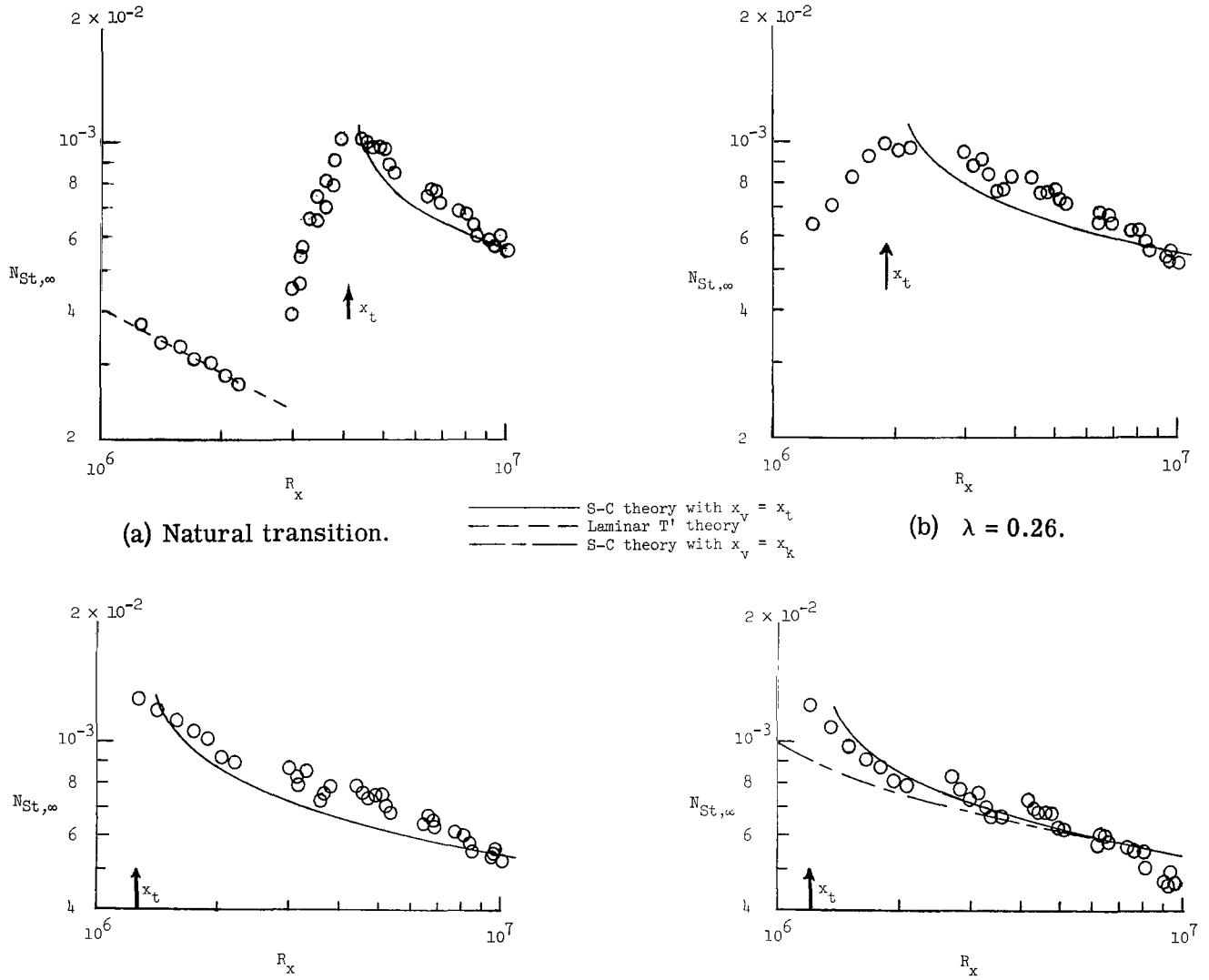

Figure 9.- Measured heat-transfer distributions downstream of jets for various injection rates at Mach 6.0. $R_{x,k} = 0.62 \times 10^6$; $x_k = 2.54$ cm; $T_w/T_t = 0.57$.

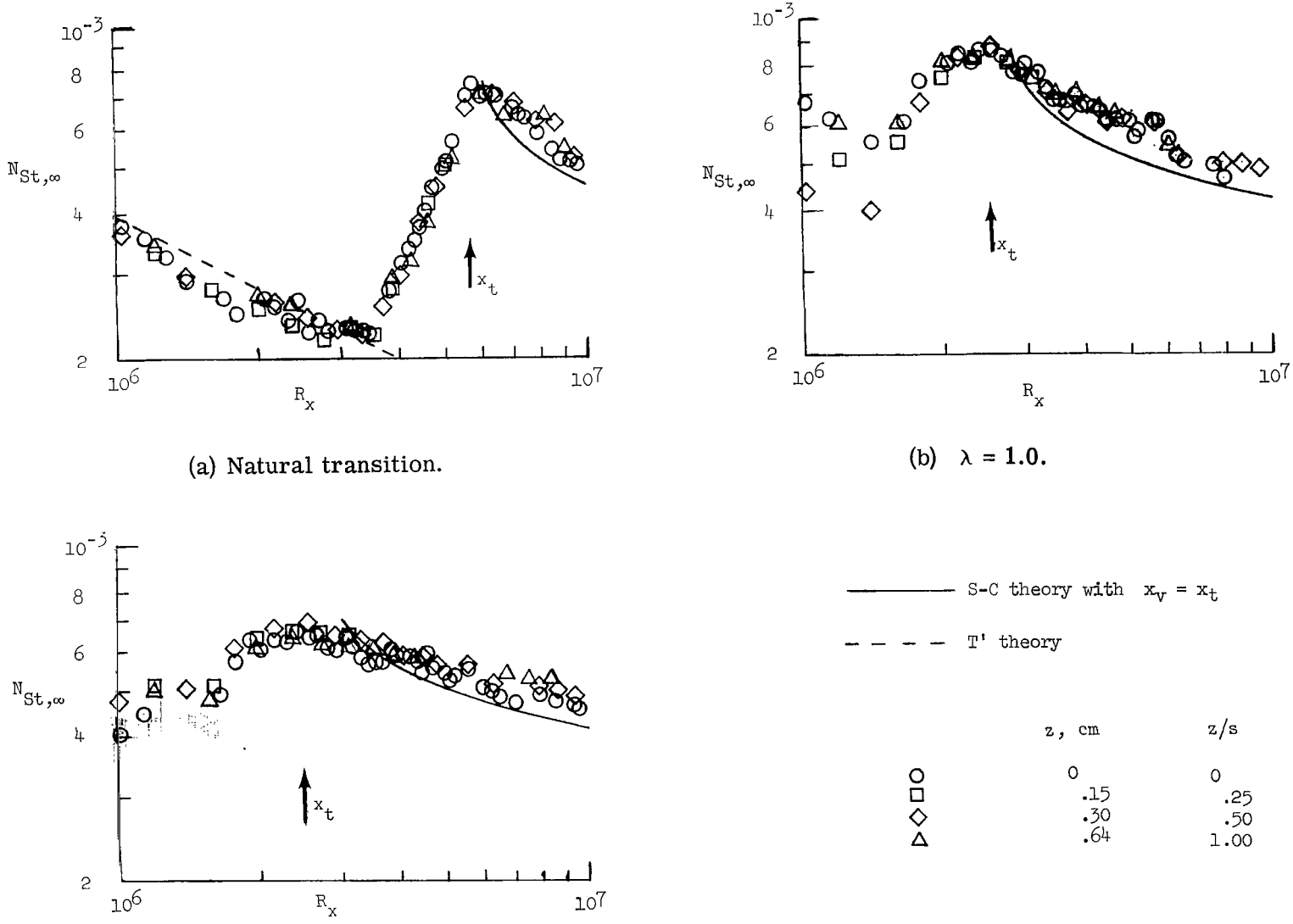

(a) Natural transition.

(b) $\lambda = 1.0$.

(c) $\lambda = 4.46$.

Figure 10.- Measured heat-transfer distributions downstream of jets for various injection rates at Mach 8.45. $R_{x,k} = 0.51 \times 10^6$; $x_k = 2.54$ cm; $T_w/T_t = 0.40$.

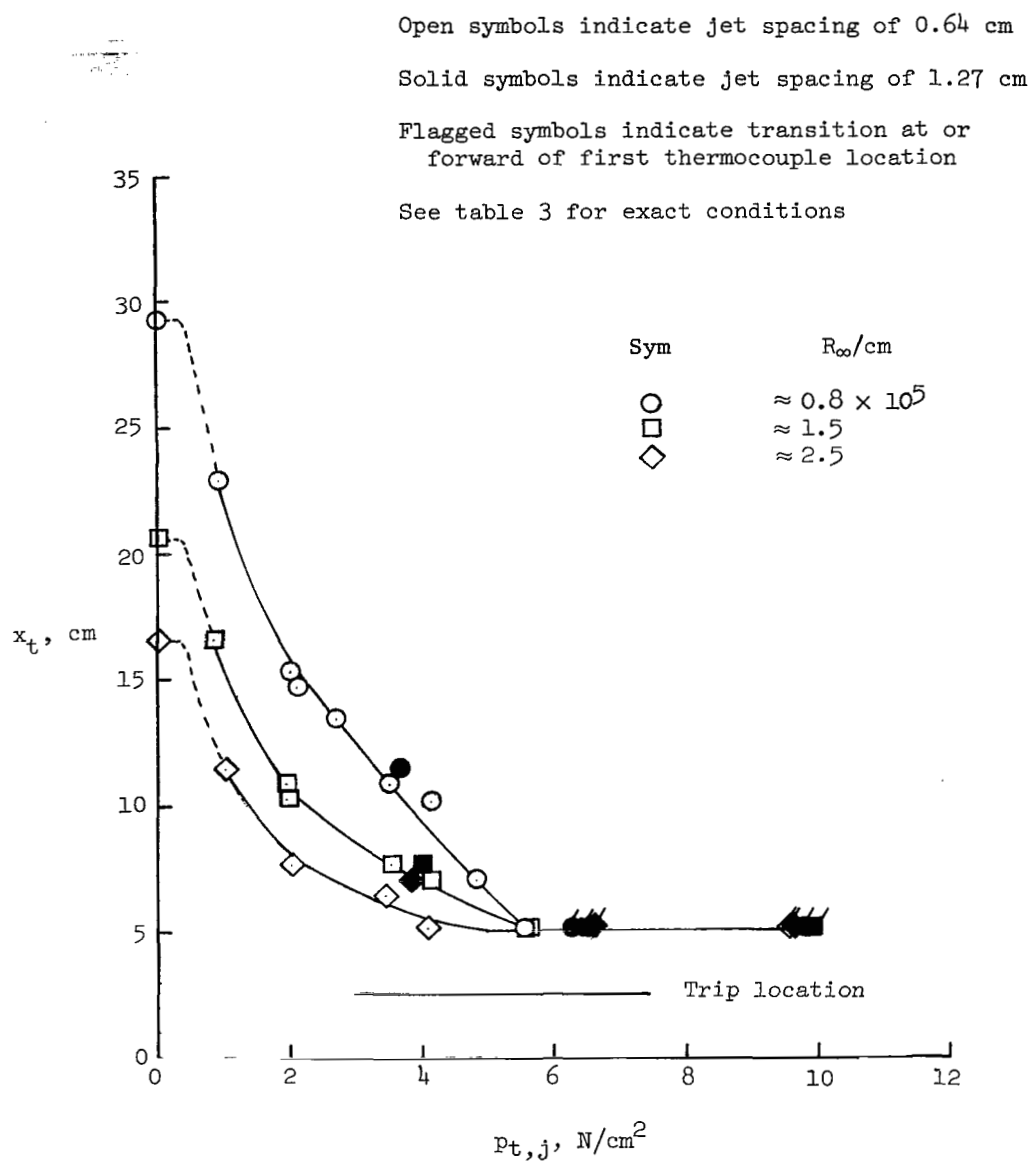

(a) Mach 6.0; $T_w/T_t = 0.57$.

Figure 11.- Movement of transition for various injection rates, trip locations, and unit Reynolds numbers.

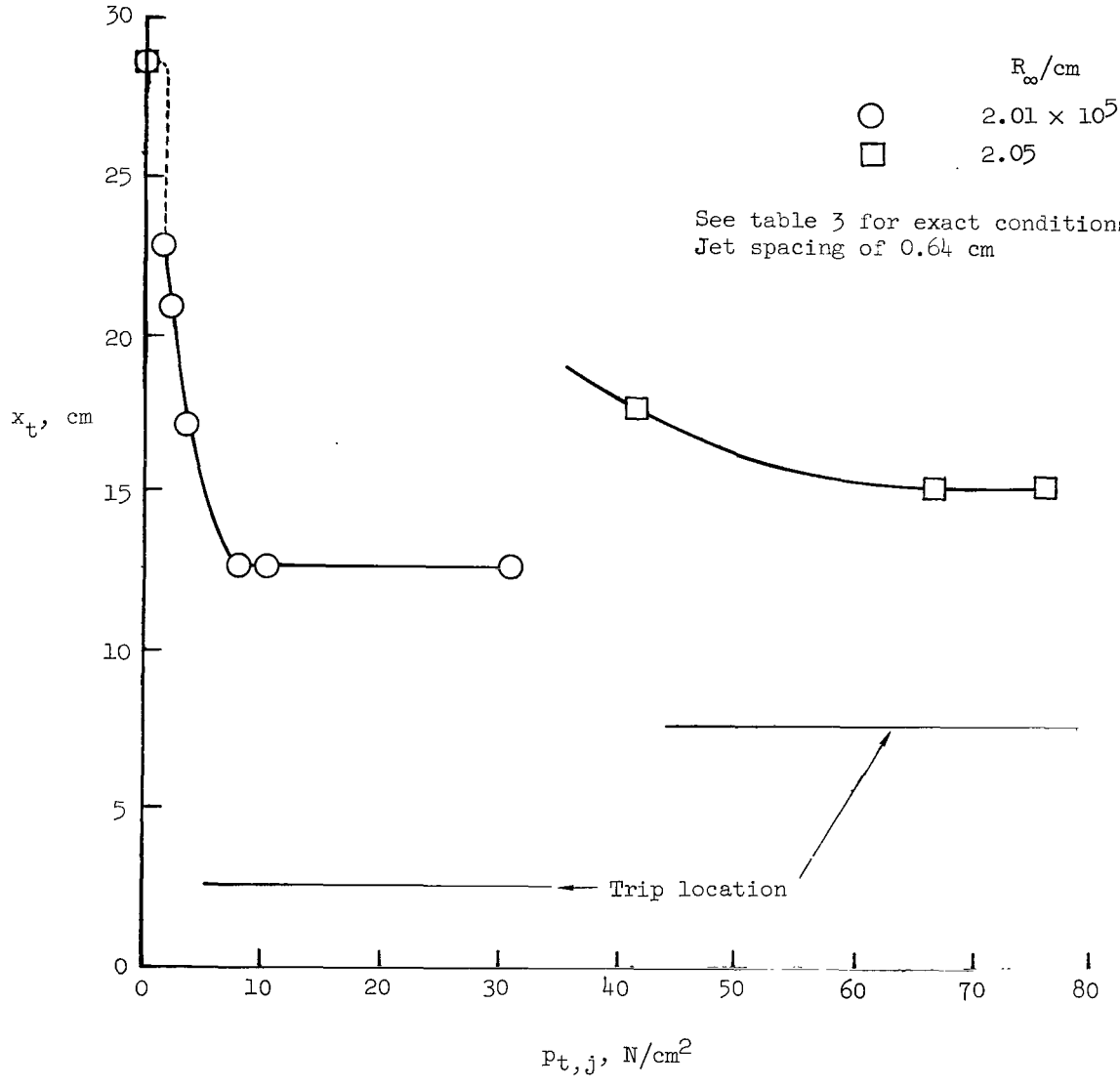

(b) Mach 8.45; $T_w/T_t = 0.4$.

Figure 11.- Concluded.

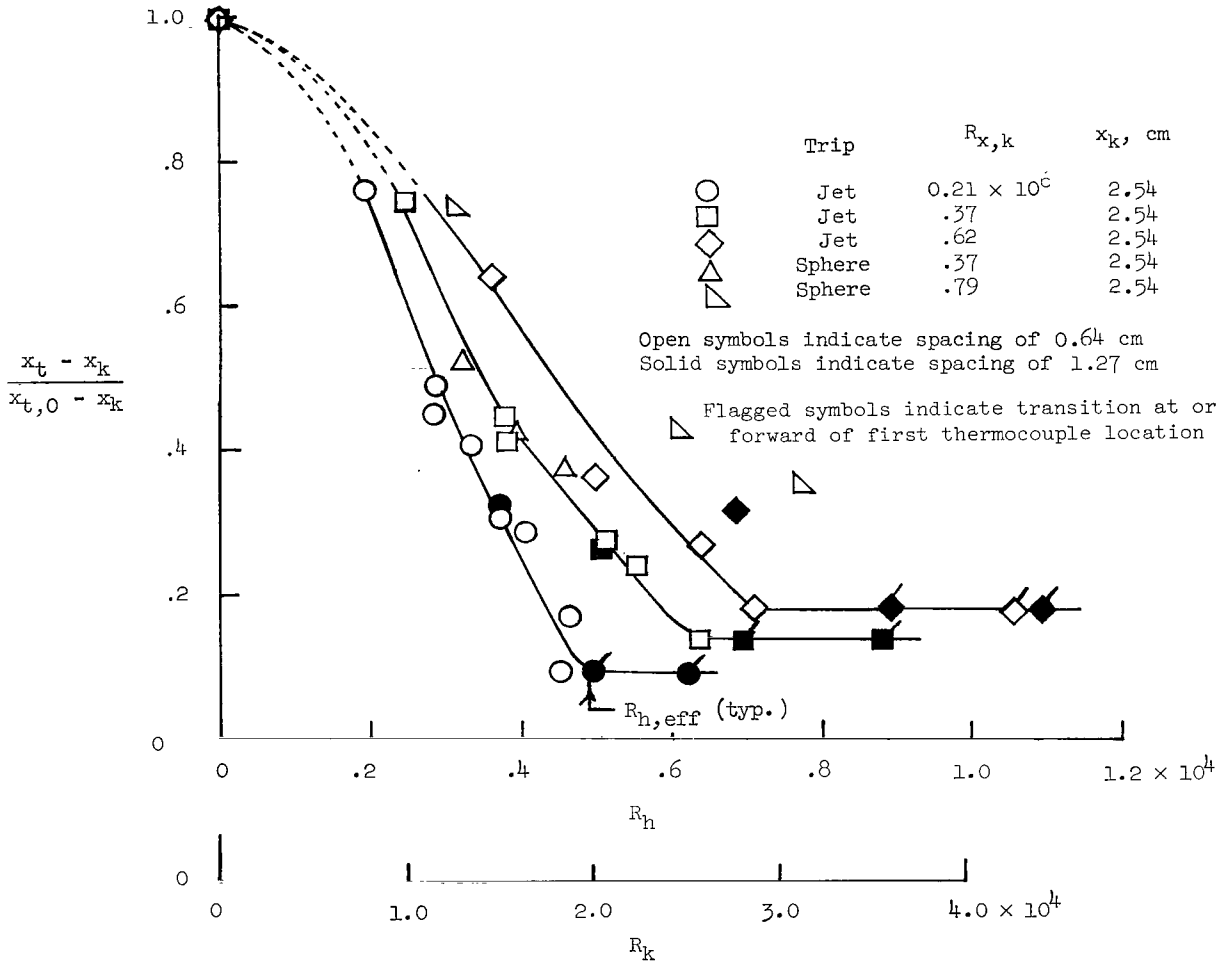

(a) Mach 6.0.

Figure 12.- Variation of jet-induced transition location with trip Reynolds number by method outlined for spherical roughness in reference 15.

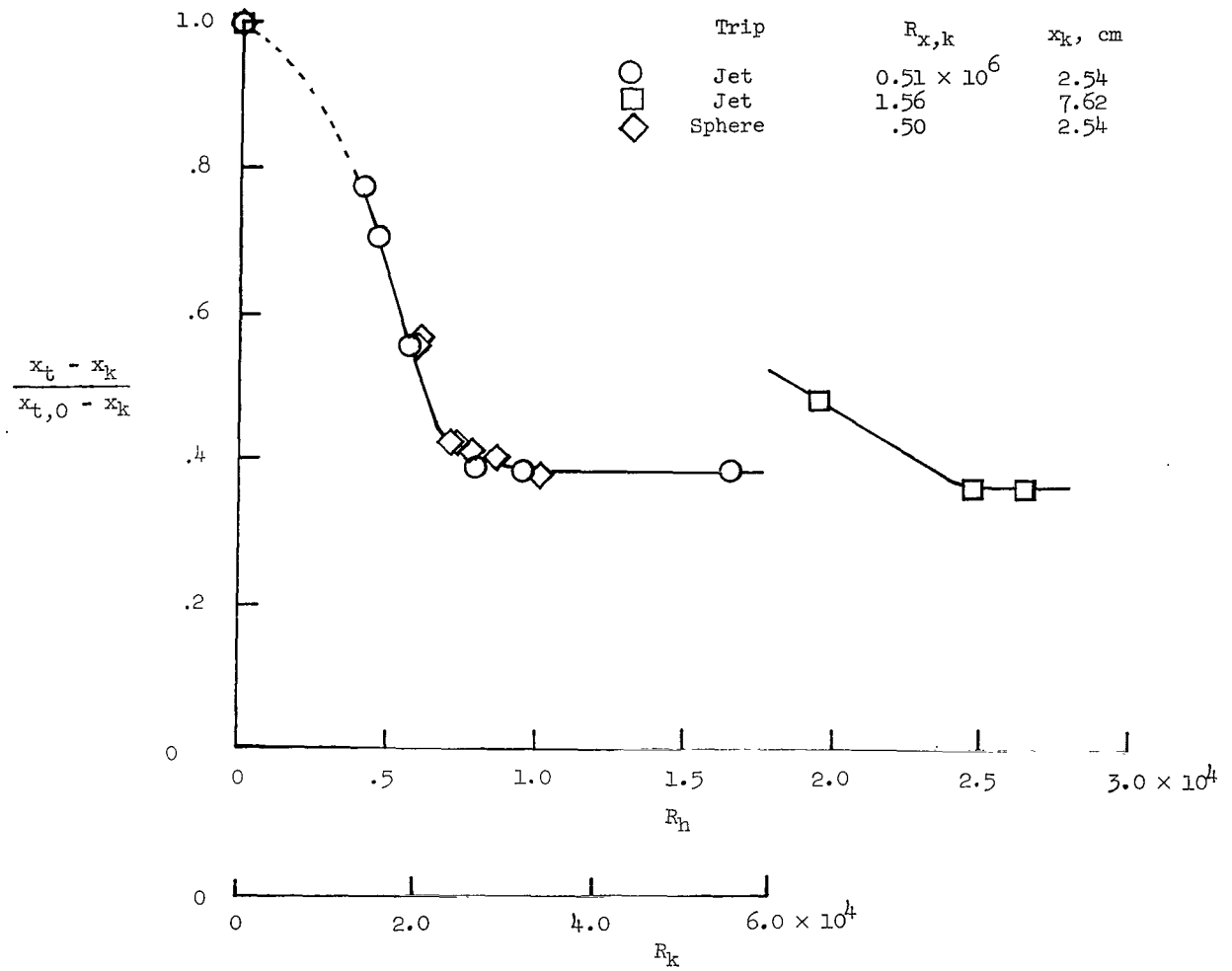

(b) Mach 8.5.

Figure 12.- Concluded.

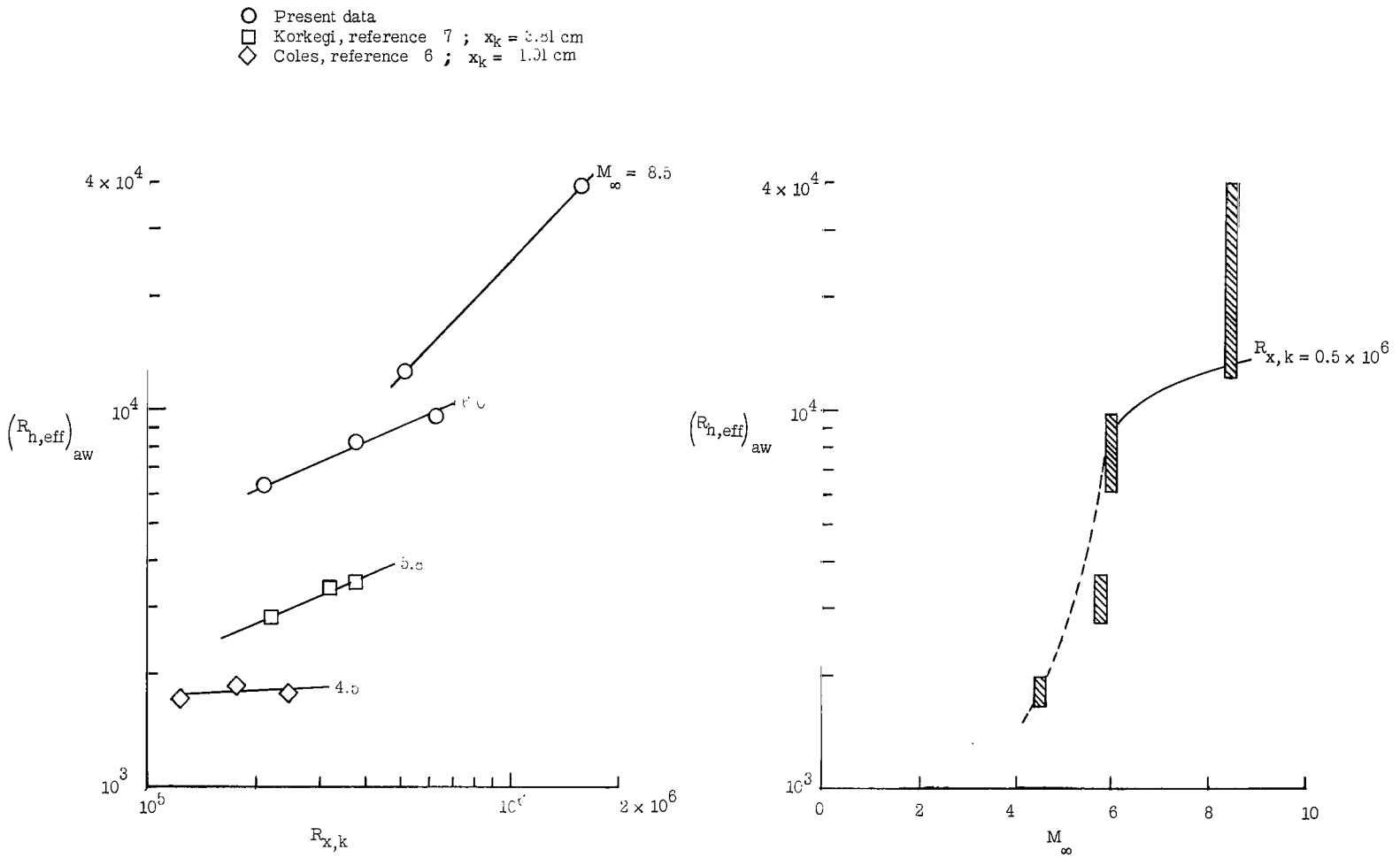

(a) Constant Mach numbers.

(b) Constant $R_{x,k}$.

Figure 13.- Variation of effective trip Reynolds number with trip-position Reynolds number and Mach number for discrete sonic jets adjusted to adiabatic wall conditions.

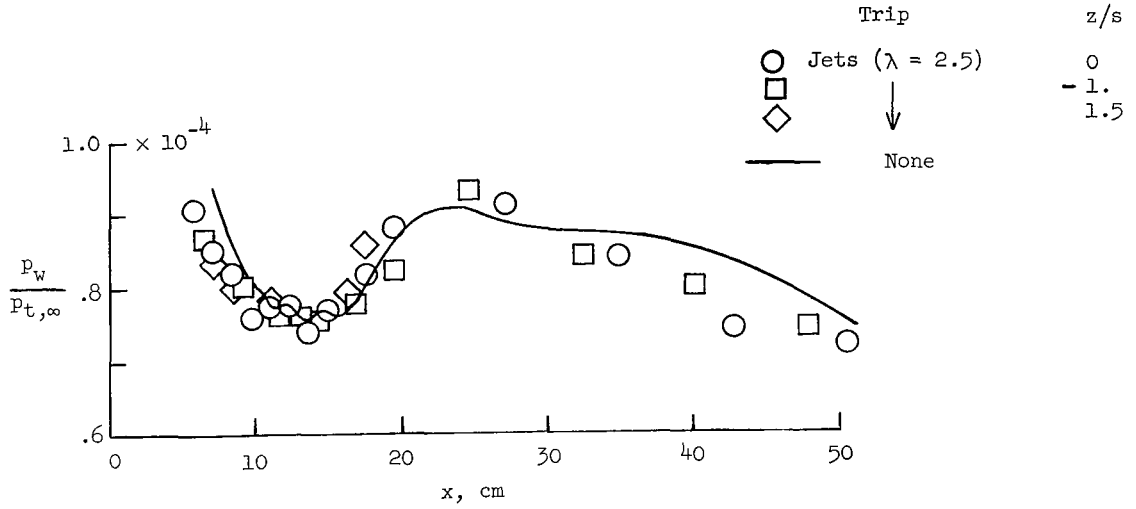

(a) Surface pressures.

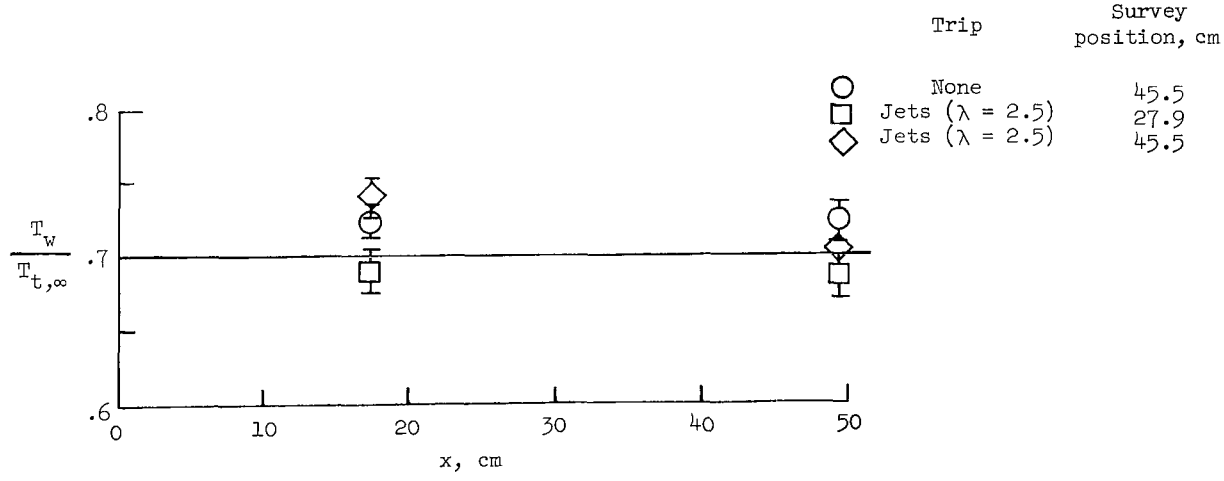

(b) Surface temperatures.

Figure 14.- Flat-plate surface conditions for surveys at Mach 8.5. $R_\infty/cm = 2.05 \times 10^5$.

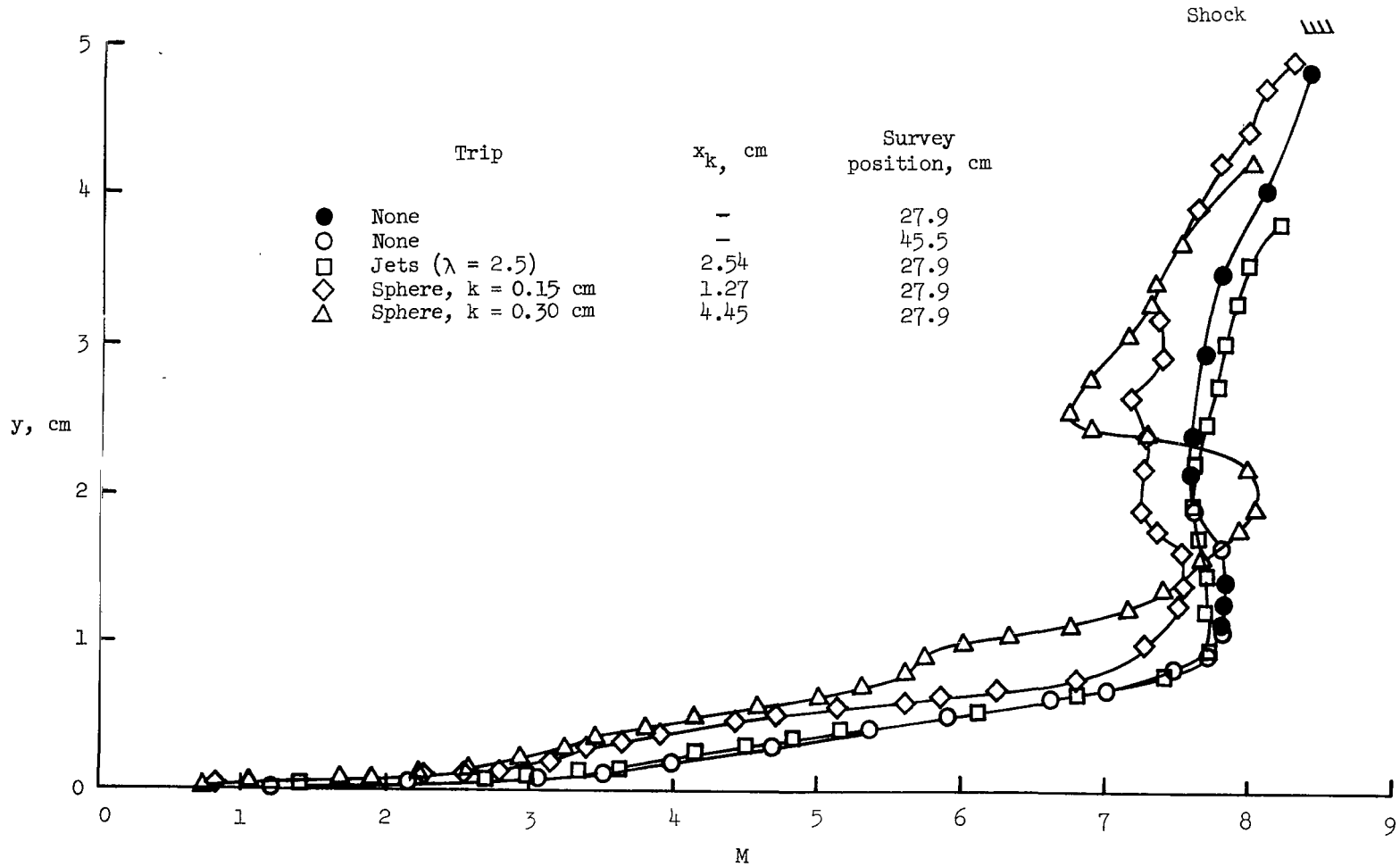

(a) $R_{x,v} \approx 3.2 \times 10^6$.

Figure 15.- Effects of effective spherical and jet trips on the downstream flow field at a free-stream Mach number of 8.5. $R_\infty/cm = 2.05 \times 10^5$; $T_w/T_t = 0.70$.

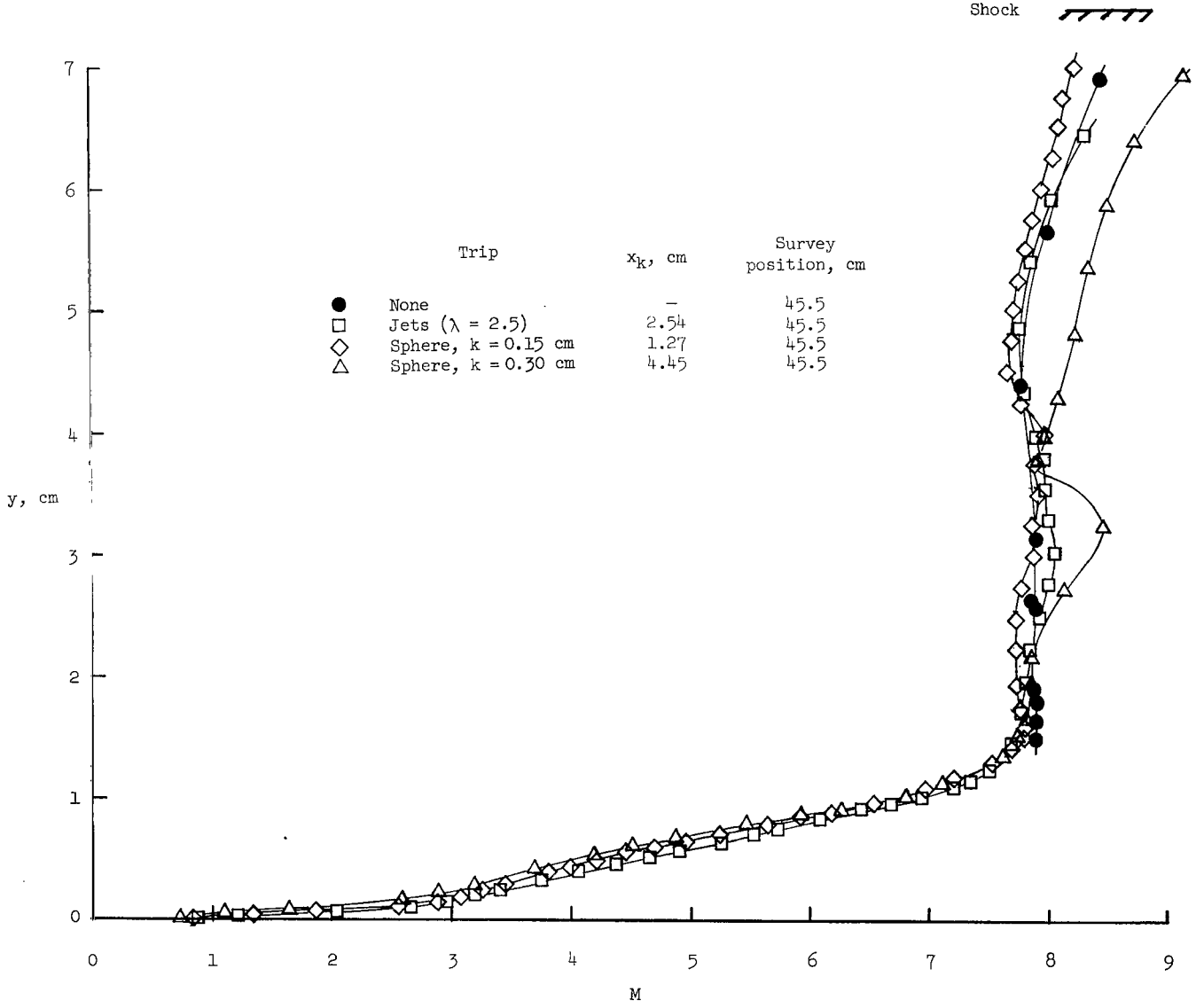

(b) $R_{x,V} = 6.8 \times 10^6$.

Figure 15.- Concluded.

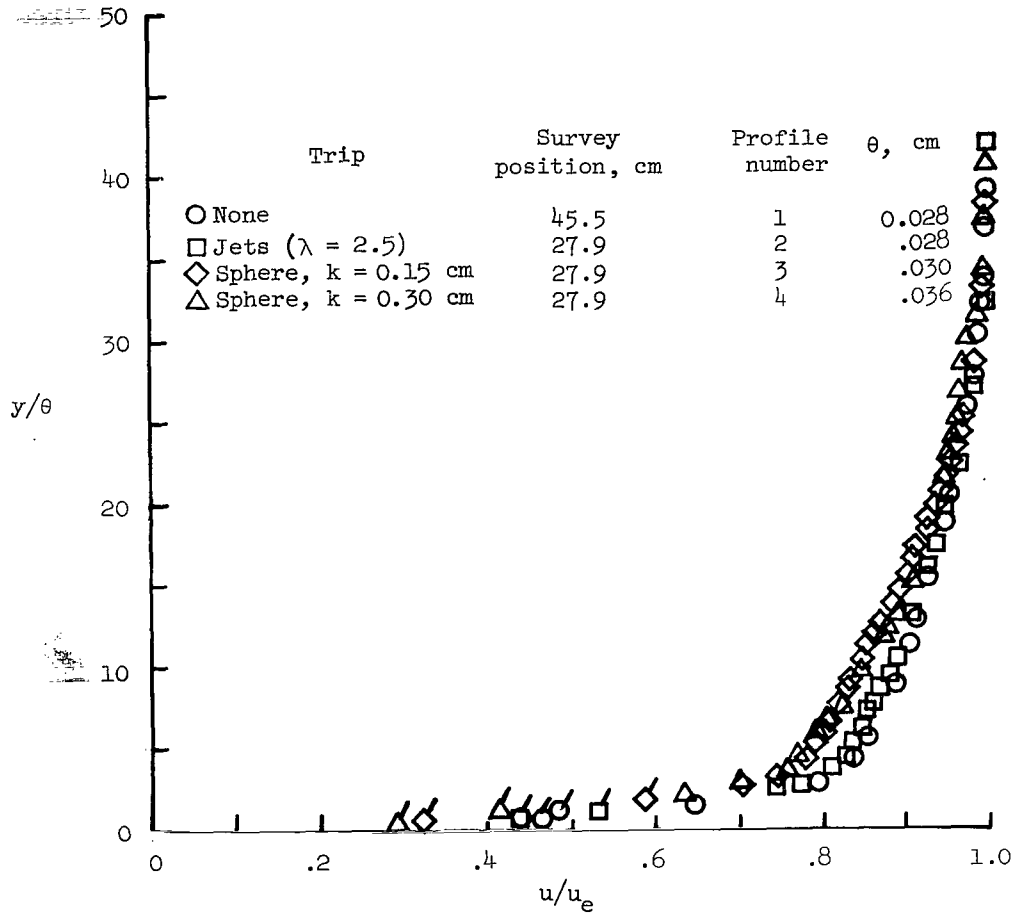

(a) $R_{x,v} \approx 3.2 \times 10^6$.

Figure 16.- Effect of trips on boundary-layer velocity profiles. All flow conditions are the same as for figure 15. Flagged symbols denote use of extrapolated values of total temperature.

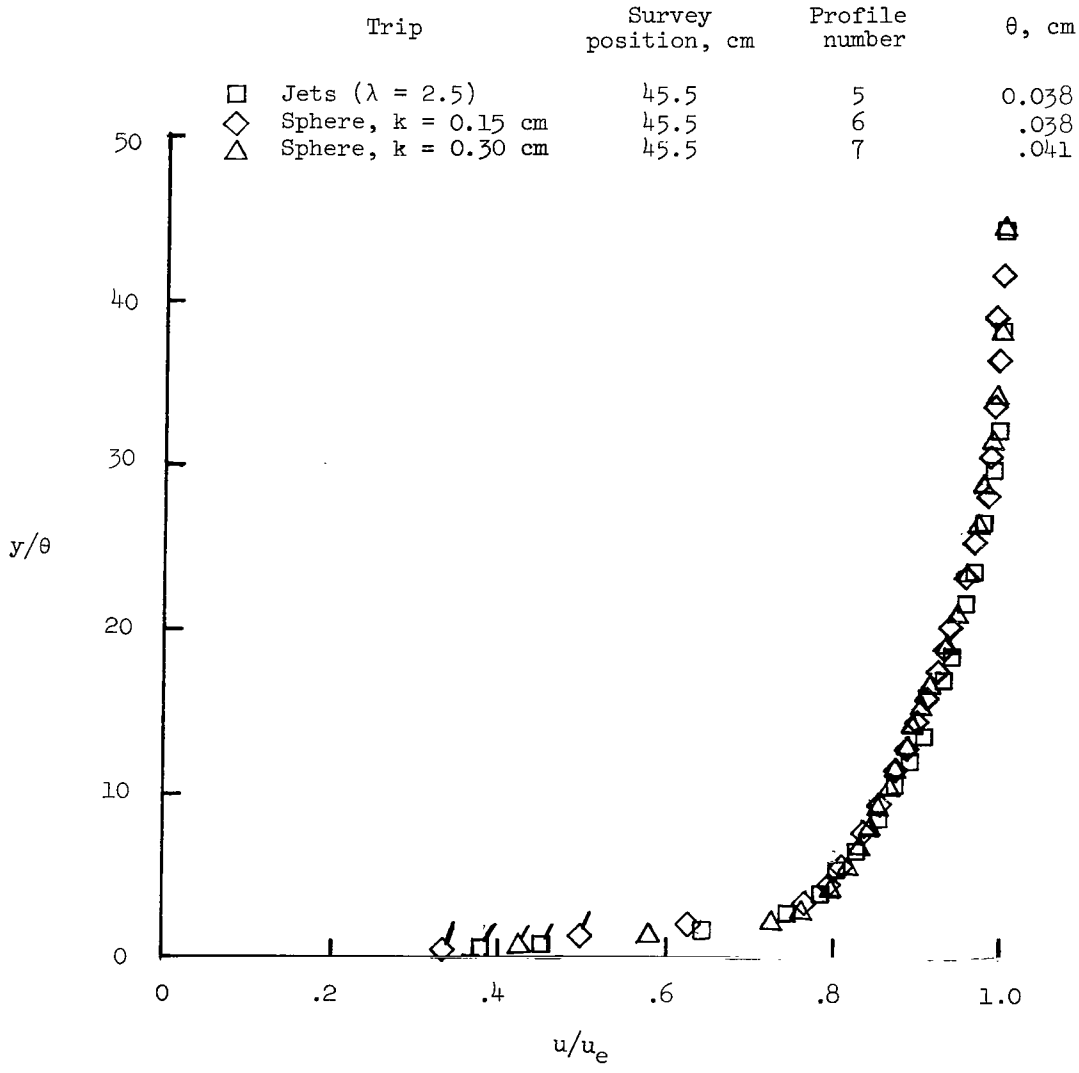

(b) $R_{x,v} \approx 6.8 \times 10^6$.

Figure 16.- Concluded.

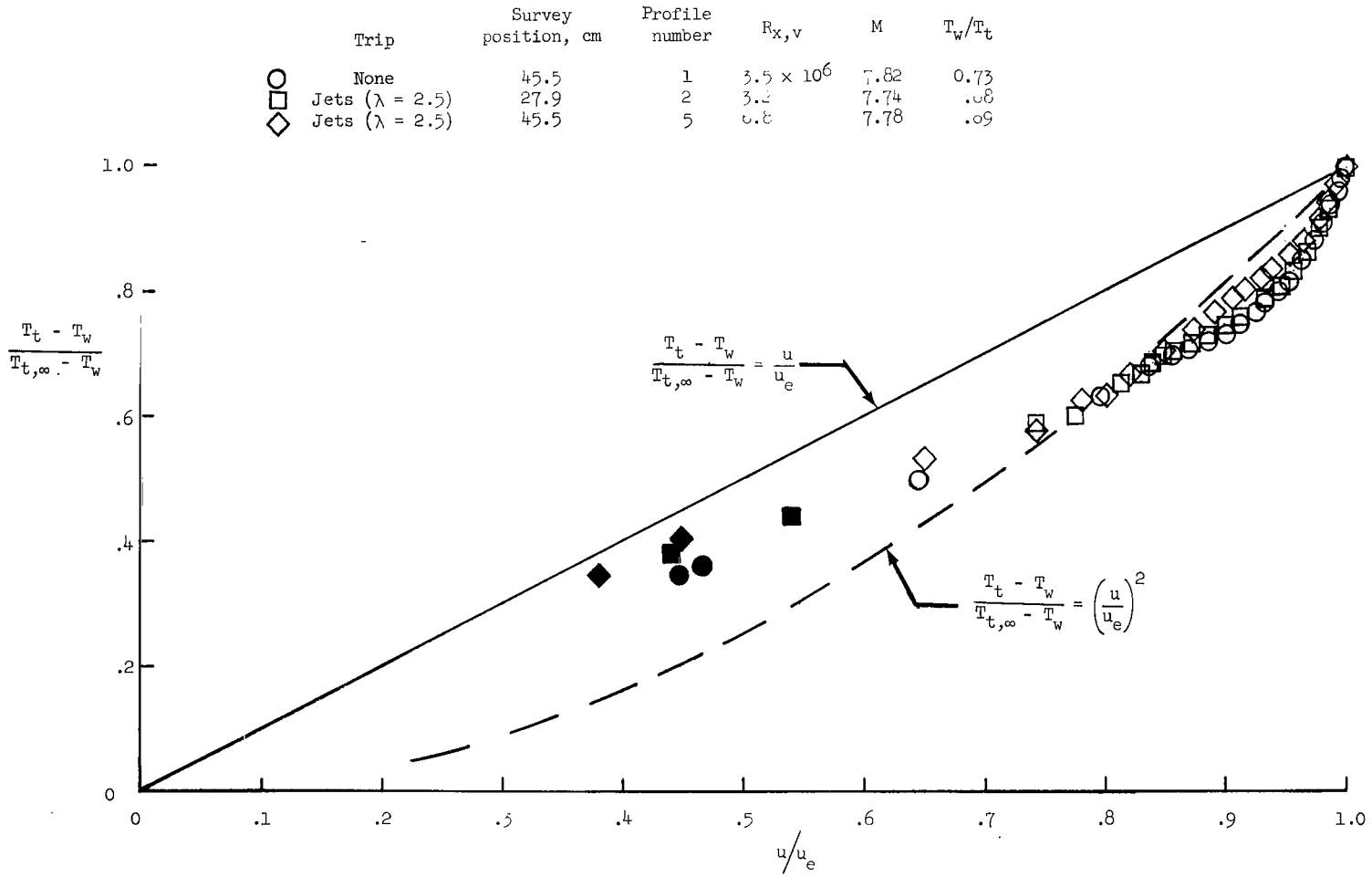

Figure 17.- Effect of jet trips on turbulent temperature-velocity relationship. Solid symbols indicate the use of extrapolated values of temperature ratio. $R_\infty/cm = 2.05 \times 10^5$.

"The aeronautical and space activities of the United States shall be conducted so as to contribute . . . to the expansion of human knowledge of phenomena in the atmosphere and space. The Administration shall provide for the widest practicable and appropriate dissemination of information concerning its activities and the results thereof."

—NATIONAL AERONAUTICS AND SPACE ACT OF 1958

NASA SCIENTIFIC AND TECHNICAL PUBLICATIONS

TECHNICAL REPORTS: Scientific and technical information considered important, complete, and a lasting contribution to existing knowledge.

TECHNICAL NOTES: Information less broad in scope but nevertheless of importance as a contribution to existing knowledge.

TECHNICAL MEMORANDUMS: Information receiving limited distribution because of preliminary data, security classification, or other reasons.

CONTRACTOR REPORTS: Scientific and technical information generated under a NASA contract or grant and considered an important contribution to existing knowledge.

TECHNICAL TRANSLATIONS: Information published in a foreign language considered to merit NASA distribution in English.

SPECIAL PUBLICATIONS: Information derived from or of value to NASA activities. Publications include conference proceedings, monographs, data compilations, handbooks, sourcebooks, and special bibliographies.

TECHNOLOGY UTILIZATION PUBLICATIONS: Information on technology used by NASA that may be of particular interest in commercial and other non-aerospace applications. Publications include Tech Briefs, Technology Utilization Reports and Technology Surveys.

Details on the availability of these publications may be obtained from:

SCIENTIFIC AND TECHNICAL INFORMATION OFFICE

NATIONAL AERONAUTICS AND SPACE ADMINISTRATION

Washington, D.C. 20546